Uniform asymptotic description of ultrashort Gaussian-pulse propagation in a causal, dispersive dielectric

Constantinos M. Balictsis
Department of Computer Science and Electrical Engineering, University of Vermont, Burlington, Vermont 05405

Kurt Edmund Oughstun
Department of Computer Science and Electrical Engineering and Department of Mathematics and Statistics, University of Vermont, Burlington, Vermont 05405

(Received 25 June 1992; revised manuscript received 2 December 1992)

The complete asymptotic description of ultrashort Gaussian-pulse propagation in a single-resonance Lorentz medium in the mature-dispersion regime is presented and compared with the results of two independent numerical experiments of the propagated-field evolution. The nonuniform asymptotic method of Olver [Stud. Appl. Math. Rev. **12**, 228 (1970)] (an extension of the method of steepest descents) is first applied to obtain the standard asymptotic description of the propagated field that is due to the given input Gaussian-modulated field. The description afforded by this asymptotic method, although nonuniform in certain space-time regions, is found to be in excellent agreement with purely numerical results, especially when exact, numerically determined saddle-point locations, and exact expressions for the derivatives of the phase function are used in the implementation of the theoretical approach. Modern uniform asymptotic techniques, which generalize Olver's nonuniform description, are then employed to obtain a rigorous description of ultrashort Gaussian-pulse propagation that is uniformly valid for all space-time points in the mature-dispersion regime. This asymptotic description clearly shows that the propagated field can be expressed solely in terms of a generalized Sommerfeld and a generalized Brillouin precursor field, the first of which dominates the total propagated field when the carrier frequency ω_c is well above resonance while the second generalized precursor field dominates when ω_c is below or near resonance. It is further shown that the pulse distortion is due solely to the manner in which the precursor field amplitude is modified by the initial Gaussian-pulse envelope spectrum. Finally, the frequency dependence of the signal velocity of the input ultrashort, Gaussian-modulated harmonic field in a single-resonance Lorentz medium is discussed.

PACS number(s): 03.40.Kf

I. INTRODUCTION

The theory of optical pulse propagation in a locally linear, homogeneous, isotropic, causally dispersive medium originated with the classical work of Sommerfeld [1] and Brillouin [2,3] concerning the propagation of an instantaneous turn-on, semi-infinite signal with monochromatic carrier wave into the half-space $z \geq 0$ occupied by a single-resonance Lorentz medium. Recently, using modern asymptotic techniques, Oughstun [4] and coworkers were able to improve significantly both the qualitative and quantitative description of this classical problem in both a single-resonance [5–7] and a double-resonance [8] Lorentz medium. Furthermore, they provided the first completely rigorous description of the dynamical field evolution of an input δ-function pulse in a single [5,6] and double-resonance [8] Lorentz medium and, more importantly, of a rectangular envelope modulated harmonic signal of fixed carrier frequency ω_c, having an arbitrary initial pulse width [9]. This recent analysis has focused on the complete precursor field evolution and the precise definition of the signal arrival, and was completely verified through precise numerical simulations [10,11]. This modern asymptotic analysis has led to a new physical description of dispersive pulse dynamics [12] that supplants the previous group-velocity description [13] in the mature-dispersion regime and reduces to it in the absence of absorption. According to this new physical description, in the mature-dispersion regime, which was found [11] to include all propagation distances z that are greater than a single absorption depth in the medium at the signal frequency, each quasimonochromatic component of the field propagates with its own characteristic velocity, which remains constant as the propagation continues. The propagated wave form is then dominated at each value of the space-time parameter $\theta = ct/z$ by a single real frequency ω_E that is the frequency of the time-harmonic field with the least attenuation that has an energy velocity [14,15] equal to z/t.

In this paper the modern asymptotic theory is applied to obtain a rigorous, uniformly valid description of ultrashort (near femtosecond) Gaussian-pulse propagation in a single-resonance Lorentz medium in the mature-dispersion regime. This is a problem of considerable practical importance due to the current experimental capability to generate ultrashort pulses approaching the femtosecond regime [16]. Furthermore, this canonical problem reduces to the previous description of an input δ-function pulse when the initial pulse width of the Gaussian envelope tends to zero, thus generalizing previous work [5–7]. The proposed theoretical description

does not rely upon any quasimonochromatic or slowly varying envelope approximations, as may be found in other descriptions [17–21], nor does it depend upon any nth-order dispersion approximation, which is central to other approaches [22,23,36], so that it rigorously maintains the causality relations [24] that are critical to the proper analysis of linear dispersive pulse propagation phenomena. These other approaches are, in a broad sense, more general in that they are typically applicable to inhomogeneous media. However, what they gain in more general applicability they lose in rigor when considering the complicated effects of dispersion and absorption on ultrashort-pulse dynamics [25–27].

The exact integral formulation describing the propagation of an arbitrary plane-wave pulse through a dispersive medium occupying the half-space $z \geq 0$ is given by [5]

$$A(z,t)=\frac{1}{2\pi}\mathrm{Re}\left\{\int_C \tilde{f}(\omega)\exp\left[\frac{z}{c}\phi(\omega,\theta)\right]d\omega\right\} \tag{1.1}$$

for all $z \geq 0$, where

$$\tilde{f}(\omega)=\int_{-\infty}^{+\infty} f(t)e^{i\omega t}dt \tag{1.2}$$

is the temporal Fourier spectrum of the initial pulse $f(t)=A(0,t)$ on the plane $z=0$. Here $A(z,t)$ represents either the scalar potential or any scalar component of the electric field, magnetic field, Hertz vector, or vector potential field. Its spectral amplitude $A(z,\omega)$ satisfies the dispersive Helmholtz equation

$$[\nabla^2+\tilde{k}^2(\omega)]A(z,\omega)=0\ , \tag{1.3}$$

with complex wave number

$$\tilde{k}(\omega)=\frac{\omega}{c}n(\omega)\ . \tag{1.4}$$

Here c denotes the vacuum speed of light and $n(\omega)=\epsilon^{1/2}(\omega)$ is the complex index of refraction (in cgs units) of the dispersive medium occupying the half-space $z \geq 0$ with complex-valued dielectric permittivity $\epsilon(\omega)$ and magnetic permeability $\mu=1$. The dispersive dielectric medium is taken here as a single resonance Lorentz medium with complex index of refraction

$$n(\omega)=\left[1-\frac{b^2}{\omega^2-\omega_0^2+i2\delta\omega}\right]^{1/2}\ . \tag{1.5}$$

Here $b^2=4\pi Ne^2/m$ is the square of the plasma frequency of the medium, N is the number density of electrons of charge e and mass m that are harmonically bound with the undamped resonance frequency ω_0, and δ is the associated phenomenological damping constant. The Lorentz model is appropriate because it is a causal model, the complex index of refraction given in Eq. (1.5) satisfying the Kramers-Krönig relations [24]. The medium parameters that were originally chosen by Brillouin [2,3] are used for the examples considered in this paper, viz., $\omega_0=4.0\times10^{16}$/sec, $b^2=20.0\times10^{32}$/sec^2, and $\delta=0.28\times10^{16}$/sec. The same set of medium parameters has also been used in recent research [4–12].

If $f(t)=0$ for all $t<0$, then the integral appearing in Eq. (1.2) is the Laplace transform of the initial time behavior of the field at $z=0$. The contour of integration C appearing in Eq. (1.1) is then the straight line $\omega=\omega'+i\alpha$ with α being a fixed positive constant that is greater than the abscissa of absolute convergence [28] for the function $f(t)$, and where $\omega'=\mathrm{Re}\{\omega\}$ ranges from negative to positive infinity. The complex phase function $\phi(\omega,\theta)$ that appears in the integral representation (1.1) is defined as

$$\frac{z}{c}\phi(\omega,\theta)=i[\tilde{k}(\omega)z-\omega t]=\frac{z}{c}i\omega[n(\omega)-\theta]\ , \tag{1.6}$$

where

$$\theta=\frac{ct}{z} \tag{1.7}$$

is a dimensionless space-time parameter such that for any distance of propagation z the important properties of the propagated field evolution occur when $\theta \geq 1$ since $A(z,t)$ identically vanishes for $\theta<1$ when $f(t)=0$ for all negative time [4,5].

A case of particular importance to this research is that of an input pulse-modulated harmonic signal of applied signal frequency ω_c that may be represented as

$$f(t)=u(t)\sin(\omega_c t+\psi)\ , \tag{1.8}$$

where $u(t)$ is the real-valued initial envelope function of the pulse and ψ is a constant phase term that is chosen to be $\pi/2$ for a cosine wave or zero for a sine wave. If $\tilde{u}(\omega)$ is the temporal Fourier transform of the initial pulse envelope, then the propagated field may be written [5] as

$$A(z,t)=\frac{1}{2\pi}\mathrm{Re}\left\{i\exp\{-i\psi\}\int_{i\alpha-\infty}^{i\alpha+\infty}\tilde{u}(\omega-\omega_c)\times\exp\left[\frac{z}{c}\phi(\omega,\theta)\right]d\omega\right\}\ . \tag{1.9}$$

The initial field envelope for the canonical problem treated in this paper is taken as the Gaussian envelope function

$$u(t)=\exp\left[-\left[\frac{t-t_0}{T}\right]^2\right] \tag{1.10}$$

that is centered around the time $t_0>0$ with a full width at e^{-1} maximum given by $2T$. The spectrum of this initial pulse envelope is then

$$\tilde{u}(\omega)=\pi^{1/2}T\exp\left\{-\frac{T^2\omega^2}{4}\right\}\exp\{i\omega t_0\}\ . \tag{1.11}$$

The exact integral representation of the propagated pulse in the dispersive medium is then given by

$$A(z,t)=\frac{1}{2\pi}\mathrm{Re}\left\{i\int_{i\alpha-\infty}^{i\alpha+\infty}\tilde{U}(\omega-\omega_c)\times\exp\left\{\frac{z}{c}\phi(\omega,\theta')\right\}d\omega\right\} \tag{1.12}$$

for $z \geq 0$, where the spectral function

$$\tilde{U}(\omega-\omega_c)=\exp\{-i(\omega t_0+\psi)\}\tilde{u}(\omega-\omega_c)$$
$$=\exp\{-i\psi\}\left[\pi^{1/2}T\exp(-i\omega_c t_0)\times\exp\left\{-\frac{T^2(\omega-\omega_c)^2}{4}\right\}\right] \quad (1.13)$$

has been introduced here for notational convenience, and where

$$\theta'=\theta-\frac{ct_0}{z}=\frac{c}{z}(t-t_0)\ . \quad (1.14)$$

Unlike the previous canonical problems [4–9] that have been treated using the asymptotic theory, the present field does not identically vanish for $\theta'<1$. However, for a sufficiently short initial pulse width $2T$ one can always choose t_0 sufficiently large such that the physically important properties of the field evolution occur when $\theta'>1$ (otherwise an analysis of the pulse dynamics for $\theta'<1$ is required).

It is clearly desirable to have two independent methods of numerically evaluating the propagated field evolution in the dispersive medium. Their agreement with each other provides a high degree of assuredness in the accuracy of their results. This then provides a well-defined set of results with which the asymptotic theory may be compared. One such experimental approach is a numerical evaluation of the integral representation (1.12) that is based on the algorithm developed by Hosono [30] for the inversion of Laplace transform-type integrals. In an improvement of this method, Wyns, Foty, and Oughstun [10] and Oughstun, Wyns, and Foty [11] were able to completely verify the predictions of the asymptotic theory concerning the propagation of an input δ-function pulse as well as a unit-step-function modulated harmonic signal through a Lorentz-type medium. For an input unit amplitude, ultrashort Gaussian-modulated pulse that is centered around a point t_0 that is equal to only a few initial pulse widths, the field is negligible for $t<0$ and thus, to an excellent degree of approximation, the representation (1.12) may be approximated as a Laplace transform-type integral. If one replaces $-i\omega$ by $s=\sigma-i\omega$ in Eq. (1.1) it can be rewritten as

$$A(z,t)=\mathrm{Re}\left\{\frac{1}{2\pi i}\int_{C_{\mathrm{Br}}}A(0,s)\exp\{i\tilde{k}(is)z\}e^{st}ds\right\}, \quad (1.15)$$

where C_{Br} denotes the appropriate Bromwich contour for an input Gaussian pulse, and where, for the Lorentz-type medium of interest here, the complex index of refraction is now of the form

$$\tilde{k}(is)=\frac{is}{c}\left[1+\frac{b^2}{s^2+2\delta s+\omega_0^2}\right]^{1/2}. \quad (1.16)$$

The numerical evaluation of the Laplace transform-type integral representation (1.15), for the particular case of Gaussian-pulse propagation treated in this paper, then proceeds directly along the lines presented in Ref. [10].

The numerical experiment may also be based on a numerical implementation of the more physically appealing method of steepest descents [8,31]. At any given value of the space-time parameter $\theta\geq 1$ the dominant contribution to the integral appearing in Eq. (1.1) is due to the dominant saddle point, which exhibits the last exponential decay, of the complex phase function $\phi(\omega,\theta)$ once the original contour of integration C has been deformed to an appropriate Olver-type path $P(\theta)$ with respect to the saddle points of $\phi(\omega,\theta)$. The original integral along C, which gives $A(z,t)$, is related to the path integral along $P(\theta)$ by the sum of the residues of any poles of $\tilde{f}(\omega)$ that are crossed in this deformation (a detailed description of this procedure may be found in Sec. 4 A of Ref. [5]). If $P(\theta)$ is chosen to be along a portion of the path of steepest descents in some specified region about each appropriate saddle point, then for a sufficiently large value of the propagation distance z the problem is reduced to a numerical integration along only that portion of the path of steepest descents in the vicinity of each appropriate saddle point, the integration along the remainder of $P(\theta)$ being exponentially negligible [8]. Notice further that $\exp\{(z/c)\phi(\omega,\theta)\}$ is nonoscillatory along the path of steepest descent so that the required numerical integration along each steepest-descent path component from each relevant saddle point may be easily accomplished with great accuracy. This numerical integration procedure is uniformly valid in the space-time parameter θ for any physically realizable input pulse shape, and is extremely efficient when the propagation distance z is large in comparison with the e^{-1} absorption depth for the frequency component considered. The only complexity involved is the numerical evaluation of the steepest-descent path segments through the relevant saddle points at each value of θ. This minor difficulty is far outweighed by the inherent accuracy of this numerical integration procedure.

For Gaussian-pulse propagation the spectral function $\tilde{U}(\omega-\omega_c)$ given in Eq. (1.13) is an analytic function in the complex ω plane so that the integral representation of the propagated field in Eq. (1.12) may be rewritten as

$$A(z,t)=\frac{T}{\pi^{1/2}}\mathrm{Re}\left[\int_{P^+(\theta')}\left[\exp\left\{-\frac{T^2[\omega^2+\omega_c^2]}{4}\right\}\cosh\left\{\frac{T^2\omega\omega_c}{2}-i\left[\omega_c t_0+\psi-\frac{\pi}{2}\right]\right\}\right]\exp\left\{\frac{z}{c}\phi(\omega,\theta')\right\}d\omega\right], \quad (1.17)$$

where $P^+(\theta')$ is the appropriate Olver-type path in the right half of the complex ω plane, and where

$$\phi(\omega,\theta')=i\omega[n(\omega)-\theta'] , \tag{1.18}$$

with θ' given by Eq. (1.14). The asymptotic method of steepest descents may now be applied (either analytically or numerically) only with respect to the saddle points of the complex phase function $\phi(\omega,\theta')$ in the right half of the complex ω plane.

II. NONUNIFORM ASYMPTOTIC DESCRIPTION OF THE PROPAGATED FIELD

In order to perform the asymptotic analysis of the integral representation given in Eq. (1.1) for the propagated field in a single-resonance Lorentz medium, it is necessary to determine the locations of the saddle points of the complex phase function $\phi(\omega,\theta)$ in the complex ω plane, as well as the value of $\phi(\omega,\theta)=X(\omega,\theta)+iY(\omega,\theta)$ at each of these critical points. Furthermore, it is essential to determine the regions of the complex ω plane wherein the real part of the complex phase function $X(\omega,\theta)=\mathrm{Re}\{\phi(\omega,\theta)\}$ is less than the value of $X(\omega,\theta)$ at the dominant saddle point (i.e., the saddle point that exhibits the least exponential decay) for a given value of θ. For a single-resonance Lorentz medium both the complex phase function $\phi(\omega,\theta)$ and the complex index of refraction $n(\omega)$ are analytic functions everywhere in the complex ω plane except for along the two branch cuts $\omega'_-\omega_-$ and $\omega_+\omega'_+$ in the lower half of the complex ω plane, where

$$\omega'_\pm=\pm(\omega_1^2-\delta^2)^{1/2}-i\delta , \tag{2.1a}$$

$$\omega_\pm=\pm(\omega_0^2-\delta^2)^{1/2}-i\delta \tag{2.1b}$$

are the branch points of $n(\omega)$, with $\omega_1^2=\omega_0^2+b^2$.

Unlike previously treated cases [1–12], the propagated field does not identically vanish for all $\theta'<1$ for Gaussian-pulse propagation so that this case must now be examined. The numerically determined saddle-point locations at several values of $\theta'<1$ are illustrated in Fig. 1. As θ' increases from negative infinity two pairs of saddle points are found to emanate from the branch points $\omega_\pm$, and these are the only saddle points of $\phi(\omega,\theta')$ for $\theta'<1$. Two first-order saddle points always lie in the lower half of the complex ω plane for $\theta'<1$. They are symmetrically situated about the imaginary axis for $\theta'<\theta_{lc}$ and approach each other as θ' increases. They coalesce into a single second-order saddle point on the imaginary axis at $\theta'=\theta_{lc}$ ($\cong 0.931\,82$ for Brillouin's choice of the medium parameters), after which they move away from each other along the imaginary axis as θ' approaches unity from below. In order to be consistent with the notation used in previous work [4–7] when $\theta'>1$, the lower saddle point that is moving towards the origin after the coalescence at $\theta'=\theta_{lc}$ is called the lower near saddle point and is denoted by SP_2, while the lower saddle point that is moving towards $-i\infty$ after the coalescence at $\theta'=\theta_{lc}$ is called the lower distant saddle point and is denoted by SP_D^-. At $\theta'=1$ the lower distant saddle-point location changes discontinuously from $0-i\infty$ as θ' tends to unity from below to the point $-\infty-i2\delta$ approached as θ' tends to unity from above. The relative locations of the lower saddle points before ($\theta'<\theta_{lc}$) and after ($\theta'>\theta_{lc}$) coalescence are clearly evident in Fig. 1. The other two first-order saddle points always lie in the upper half of the complex ω plane for $\theta'<1$. They are symmetrically situated about the imaginary axis for $\theta'<\theta_{uc}$ and approach each other as θ' increases. They coalesce into a single second-order saddle point on the imaginary axis at $\theta'=\theta_{uc}$ ($\cong 0.945\,14$ for Brillouin's choice of the medium parameters), after which they move away from each other along the imaginary axis as θ' tends to unity from below. Again, in order to be consistent with the notation used in previous work [4–7] when $\theta'>1$, the upper saddle point that is moving towards the origin after the coalescence is called the upper near saddle point and is denoted by SP_1, while the second upper saddle point that is approaching $+i\infty$ after the coalescence is called the upper distant

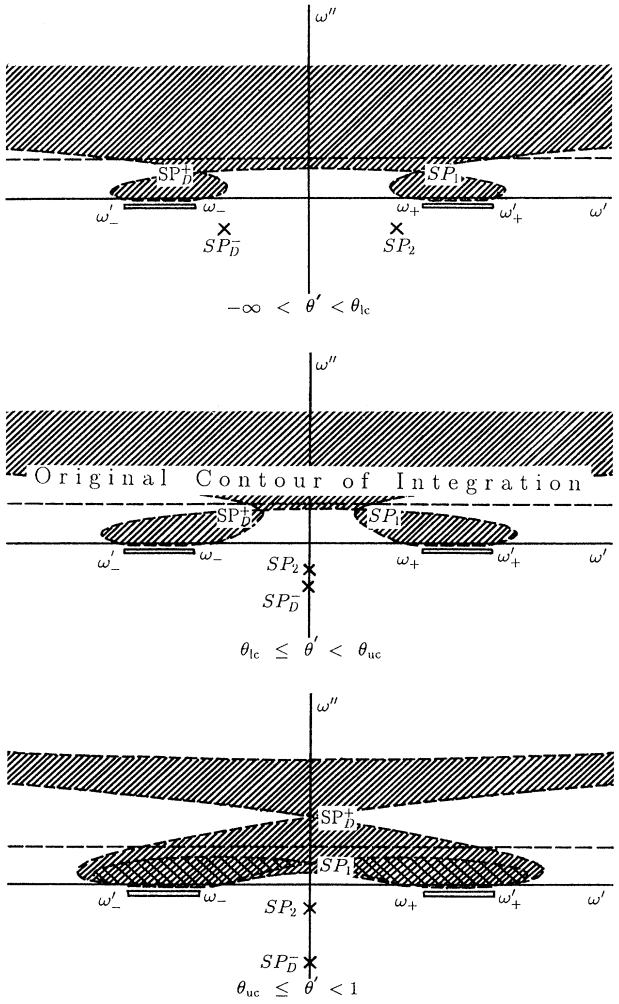

FIG. 1. Dynamic behavior of the saddle points and the real part of the complex phase function $X(\omega,\theta')=\mathrm{Re}\{\phi(\omega,\theta')\}$ for $-\infty<\theta'<1$. The dashed contours indicate the isotimic contours of $X(\omega,\theta')$ through the relevant saddle points, and the shaded areas indicate the regions of the complex ω plane wherein $X(\omega,\theta')$ is less than that at these points.

saddle point and is denoted by SP_D^+. The upper distant saddle-point location changes discontinuously from the point $0+i\infty$ as θ' tends to unity from below to the point $+\infty-i2\delta$ approached as θ' tends to unity from above. The relative locations of the upper saddle points before ($\theta'<\theta_{uc}$) and after ($\theta'>\theta_{uc}$) coalescence are clearly evident in Fig. 1.

Upon turning attention to the saddle-point dominance for $\theta'<1$, it is found from numerical calculations that the two lower saddle points are dominant over the two upper saddle points for all $\theta'<1$. In particular, for increasing values of θ' from negative infinity and up until θ_{lc}, the two lower saddle points have the same dominance [i.e., the value of $X(\omega,\theta')$ is the same at both of them], after which for increasing values of $\theta'>\theta_{lc}$ up to unity the lower near saddle point SP_2 is dominant over the lower distant saddle point SP_D^- [i.e., $X(\omega_{SP_2},\theta')>X(\omega_{SP_D^-},\theta')$]. The two upper saddle points have the same dominance up until θ_{uc}, after which and for increasing values of $\theta'>\theta_{uc}$ up to unity, the upper distance saddle point SP_D^+ is dominant over the upper near saddle point SP_1. A further numerical study of the isotomic contours of the real part of the phase function $X(\omega,\theta')$ for $\theta'<1$ revealed, as shown in Fig. 1, that the original path of integration C appearing in Eq. (1.1) cannot be deformed to an Olver-type path $P(\theta')$ with respect to the lower pair of saddle points without crossing the branch cuts $\omega'_-\omega_-$ and $\omega_+\omega'_+$ and cannot be deformed to an Olver-type path with respect to either of the upper pair of saddle points. As a consequence, the asymptotic analysis of the integral representation of the propagated field is not possible for $\theta'<1$. Although the solution to this portion of the problem would have provided a complete asymptotic description of Gaussian-pulse propagation, it is not essential to this description if t_0 is chosen sufficiently large. In that case, all of the interesting physical phenomena occur for $\theta'>1$.

For every value of $\theta'\geq 1$ except one there are again two pairs of first-order saddle points of $\phi(\omega,\theta')$ that are symmetrically situated with respect to the imaginary axis. The two so-called distance saddle points always lie in the lower half of the complex ω plane in the region $|\omega|\geq\omega_1$ above the absorption band of the Lorentz medium and move in symmetrically from $\pm\infty-i2\delta$ at $\theta'=1$ and approach the respective branch points ω'_+ and ω'_- as θ' increases to infinity. The two so-called near saddle points lie in the region $|\omega|\leq\omega_0$ below the absorption band and move along the imaginary axis symmetrically about the point $-i2\delta/3\alpha$ and approach that point as θ' approaches θ_1 from below, where they coalesce at $\theta'=\theta_1$ ($\cong 1.501$ for Brillouin's choice of the medium parameters) into a second-order saddle point, after which they move symmetrically off the imaginary axis into the lower half of the complex ω plane and approach the branch points ω_+ and ω_- as θ' tends to infinity.

Since the original path of the integration for the integral of interest given in Eq. (1.1) is not deformable through the lower near saddle point for $1\leq\theta'<\theta_1$, it is irrelevant in the present analysis throughout this θ' range. Here

$$\theta_1\cong\theta_0+\frac{2\delta^2b^2}{\theta_0\omega_0^2(3\alpha\omega_0^2-4\delta^2)}\ , \tag{2.2a}$$

with

$$\theta_0=n(0)=\left[1+\frac{b^2}{\omega_0^2}\right]^{1/2} \tag{2.2b}$$

and

$$\alpha=1-\frac{\delta^2(4\omega_1^2+b^2)}{3\omega_0^2\omega_1^2}\ . \tag{2.2c}$$

Furthermore, it was found [4,5] that the two distant saddle points $SP_D^\pm$ are equally dominant over the upper near

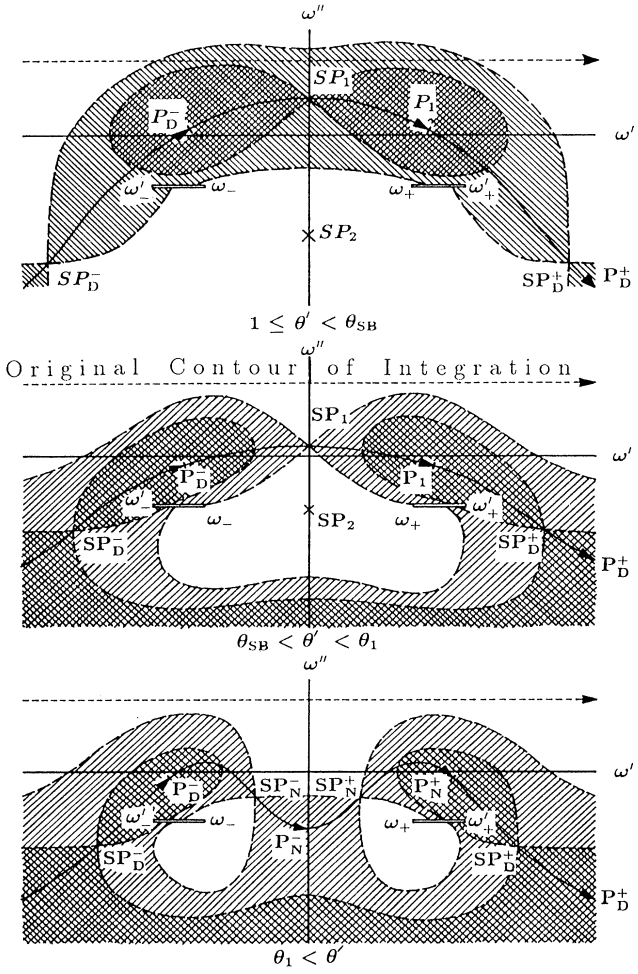

FIG. 2. Dynamic behavior of the saddle points and the real part of the complex phase function $X(\omega,\theta')=\mathrm{Re}\{\phi(\omega,\theta')\}$ for $1\leq\theta'<+\infty$. The dashed contours indicate the isotimic contours of $X(\omega,\theta')$ through the relevant saddle points, and the shaded areas indicate the regions of the complex ω plane wherein $X(\omega,\theta')$ is less than that at these points. The subpaths $P_D^\pm(\theta')$ and $P_N^\pm(\theta')$ are Olver-type paths with respect to the saddle points $SP_D^\mp$ and $SP_N^\mp$, respectively, and the subpath $P_1(\theta')$ is an Olver-type path with respect to the upper saddle point SP_1 for $1\leq\theta'\leq\theta_1$.

saddle point SP_1 for $1 \le \theta' \le \theta_{SB}$, where $\theta_{SB} \cong \theta_0 - 4\delta^2 b^2/3\theta_0\omega_0^4 \cong 1.334$ for Brillouin's choice of the medium parameters. At $\theta' = \theta_{SB}$ all three saddle points have the same dominance, after which and up until $\theta' = \theta_1$ the upper near saddle point is dominant over the two distant saddle points. For all $\theta' > \theta_1$ both near saddle points $SP_N^{\pm}$ are dominant over both of the distant saddle points $SP_D^{\pm}$.

In order to perform the asymptotic analysis of the propagated field $A(z,t)$ for large z, the integral representation of $A(z,t)$ along the original contour of integration C, as given in Eq. (1.1), must be expressed in terms of an integral $I(z,\theta')$ with the same integrand but with a new contour of integration $P(\theta')$ which is comprised of a set of Olver-type paths with respect to each of the appropriate saddle points of $\phi(\omega,\theta')$ to which the original contour of integration may be deformed. The two integral representations are then related by the sum of the residues of any poles of the initial pulse spectrum $\tilde{f}(\omega)$ that are crossed in this deformation. An example of such a path $P(\theta')$ for several values of $\theta' > 1$ is illustrated in Fig. 2.

For the particular case of Gaussian-pulse propagation the spectral function $\tilde{U}(\omega - \omega_c)$ appearing in the integral representation (1.12) of the propagated field is an analytic function in the entire complex ω plane, so that

$$A(z,t) = I(z,\theta') = \frac{1}{2\pi}\mathrm{Re}\left\{ i \int_{P(\theta')} \tilde{U}(\omega-\omega_c) \times \exp\left[\frac{z}{c}\phi(\omega,\theta')\right] d\omega \right\} \tag{2.3}$$

for all $z \ge 0$. An application of Olver's method [32] to the above integral representation then leads to the following general expression for the asymptotic approximation of the integral representation of the propagated field:

$$A(z,t) = A_S(z,t) + A_B(z,t) + R(z,\theta') , \tag{2.4}$$

which is valid for all $\theta' > 1$. By analogy with the expression for the unit-step-function signal [4–6], the term $A_S(z,t)$ is called the generalized Sommerfeld precursor because it is due to the distant saddle-point contribution and the term $A_B(z,t)$ is called the generalized Brillouin precursor because it is due to the near saddle-point contribution. An estimate of the remainder term $R(z,\theta')$ as z tends to positive infinity is obtained by taking the largest estimate of the remainder terms when the Olver-type expansions around the near and distant saddle points are performed. The important feature of Eq. (2.4) is that the asymptotic behavior of the propagated field $A(z,t)$ is expressed as the sum of two terms which are uncoupled so that they can be treated independently of one another.

A. Generalized Sommerfeld precursor

The contribution of the two distant saddle points to the asymptotic behavior of the field $A(z,t)$ for sufficiently large values of the observation distance z yields the dynamical evolution of the generalized Sommerfeld (or first) precursor field $A_S(z,t)$, which is the dominant contribution to the asymptotic behavior of the total field for all values of θ' in the range $1 \le \theta' < \theta_{SB}$. Application of Olver's theorem [32] to the integral (2.3) over the Olver-type path through each of the two distant saddle points for $\theta' > 1$ gives the general asymptotic expression for the generalized Sommerfeld precursor field as

$$A_S(z,t) = \frac{1}{2\pi}\mathrm{Re}\left\{ i \left[2\exp\left\{\frac{z}{c}\phi(\omega_{SP_D^+},\theta')\right\}\left(\frac{\pi c}{z}\right)^{1/2} a_0(\omega_{SP_D^+})[1+O(z^{-1})] + 2\exp\left\{\frac{z}{c}\phi(\omega_{SP_D^-},\theta')\right\}\left(\frac{\pi c}{z}\right)^{1/2} a_0(\omega_{SP_D^-})[1+O(z^{-1})] \right] \right\} \tag{2.5}$$

as $z \to +\infty$ uniformly for $\theta' \ge 1+\Delta$, where $\Delta > 0$. The quantity $\omega_{SP_D^{\pm}}(\theta') = \pm\xi(\theta') - i\delta(1+\eta(\theta'))$ denotes the right and left distant saddle-point locations, and the coefficients $a_0(\omega_{SP_D^{\pm}})$ are given by

$$a_0(\omega_{SP_D^{\pm}}) = \frac{\tilde{U}(\omega_{SP_D^{\pm}} - \omega_c)}{2\left[-\frac{1}{2}\frac{d^2}{d\omega^2}[\phi(\omega_{SP_D^{\pm}},\theta')]\right]^{1/2}} . \tag{2.6}$$

The proper value of the argument of the term in the square root appearing in the denominator of Eq. (2.6), as specified by the convention set forth in Olver's analysis [32], is $\pm\pi/2$ (plus for the right, and minus for the left distant saddle point). The second-order approximations to the functions $\xi(\theta')$ and $\eta(\theta')$ appearing in the distant saddle-point locations have been obtained by Oughstun [4] and Oughstun and Sherman [5,6] as

$$\xi(\theta') \cong \left[\omega_0^2 - \delta^2 + \frac{b^2\theta'^2}{\theta'^2-1}\right]^{1/2} , \tag{2.7a}$$

$$\eta(\theta') \cong \frac{(\delta^2/27) + (b^2/[\theta'^2-1])}{\xi^2(\theta')} \tag{2.7b}$$

and are reasonably accurate for all $\theta' > 1$. Substitution of these expressions into Eqs. (2.5) and (2.6) yields the approximate expression of the nonuniform asymptotic behavior of the generalized Sommerfeld precursor field for an input unit amplitude, ultrashort Gaussian-modulated harmonic signal that is presented in Ref. [29].

It is important to note again here that as the parameter θ' approaches unity from above, the two distant saddle points approach infinity and Olver's method fails. Thus

the asymptotic expression (2.5) is valid only for values of θ' bounded away from unity from above.

B. Generalized Brillouin precursor

For sufficiently large values of the observation distance z, the contribution of the near saddle points to the asymptotic behavior of the field $A(z,t)$ yields the dynamical evolution of the generalized Brillouin (or second) precursor field, denoted by $A_B(z,t)$ in Eq. (2.4). This is the dominant contribution to the total field evolution for $\theta' > \theta_{SB}$. Since the two near first-order saddle points remain separate from each other for all $\theta' \neq \theta_1$, while they coalesce into a single second-order saddle point at $\theta' = \theta_1$, Olver's theorem [32] must then be applied separately in each of the three θ' ranges $1 \leq \theta' < \theta_1$, $\theta' = \theta_1$, and $\theta' > \theta_1$.

For $1 \leq \theta' < \theta_1$ the general expression for the generalized Brillouin precursor is given by

$$A_B(z,t) = \frac{1}{2\pi} \mathrm{Re} \left[i \left[2 \exp \left\{ \frac{z}{c} \phi(\omega_{\mathrm{SP}_1}, \theta') \right\} \left[\frac{\pi c}{z} \right]^{1/2} \times a_0(\omega_{\mathrm{SP}_1}) [1 + O(z^{-1})] \right] \right] \tag{2.8}$$

as $z \to +\infty$ uniformly for $1 \leq \theta' \leq \theta_1 - \Delta$ with $0 < \Delta < \theta_1 - 1$. In Eq. (2.8) $\omega_{\mathrm{SP}_1}(\theta') = i[|\Psi(\theta')| - 2\delta\zeta(\theta')/3]$ denotes the location of the upper near saddle point, which is the only relevant saddle point in this θ' range, and the coefficient $a_0(\omega_{\mathrm{SP}_1})$ is given by

$$a_0(\omega_{\mathrm{SP}_1}) = \frac{\tilde{U}(\omega_{\mathrm{SP}_1} - \omega_c)}{2 \left[-\frac{1}{2} \frac{d^2}{d\omega^2} [\phi(\omega_{\mathrm{SP}_1}, \theta')] \right]^{1/2}} . \tag{2.9}$$

The proper value of the argument of the term appearing inside the square root in the denominator of relation (2.9) as specified by the convention in Olver's analysis [32] is equal to zero. The second approximate expressions for the functions appearing in the near saddle-point locations are given by [4–6]

$$\Psi(\theta') \cong \left[\frac{\omega_0^2(\theta'^2 - \theta_0^2)}{\theta'^2 - \theta_0^2 + \frac{3\alpha b^2}{\omega_0^2}} - \delta^2 \left\{ \frac{\theta'^2 - \theta_0^2 + \frac{2b^2}{\omega_0^2}}{\theta'^2 - \theta_0^2 + \frac{3\alpha b^2}{\omega_0^2}} \right\}^2 \right]^{1/2} , \tag{2.10a}$$

$$\zeta(\theta') \cong \frac{3 \left[\theta'^2 - \theta_0^2 + \frac{2b^2}{\omega_0^2} \right]}{2 \left[\theta'^2 - \theta_0^2 + \frac{3\alpha b^2}{\omega_0^2} \right]} . \tag{2.10b}$$

At $\theta' = c(t - t_0)/z = \theta_1$, application of Olver's theorem [32] at the second-order near saddle-point location yields the following general expression for the generalized Brillouin precursor:

$$A_B(z,t_1) = \frac{1}{2\pi} \mathrm{Re} \left[i \left[\exp \left\{ \frac{z}{c} \phi(\omega_{\mathrm{SP}_N}, \theta_1) \right\} \Gamma(\tfrac{1}{3}) \times [a_0^+(\omega_{\mathrm{SP}_N}) - a_0^-(\omega_{\mathrm{SP}_N})] \times \left[\frac{c}{z} \right]^{1/3} [1 + O(z^{-1/3})] \right] \right] \tag{2.11}$$

as $z \to +\infty$ with fixed $\theta' = \theta_1 = (ct_1/z)$, where $\omega_{\mathrm{SP}_N} \cong -i(2\delta/3\alpha)$ denotes the location of the second-order near saddle point, and where the coefficients $a_0^{\pm}(\omega_{\mathrm{SP}_N})$ are given by the expression

$$a_0^{\pm}(\omega_{\mathrm{SP}_N}) = \frac{\tilde{U}(\omega_{\mathrm{SP}_N} - \omega_c)}{3 \left[-\frac{1}{6} \frac{d^3}{d\omega^3} [\phi^{\pm}(\omega_{\mathrm{SP}_N}, \theta_1)] \right]^{1/3}} . \tag{2.12}$$

The proper value of the argument of the term appearing inside the cubic root in the denominator of relation (2.12) is $-\pi/2$ [corresponding to the plus superscript in relations (2.11) and (2.12)] along the deformed contour leading away from SP_N into the right half of the complex ω plane and $-5\pi/2$ [corresponding to the minus superscript in relations (2.11) and (2.12)] along the deformed contour leading away from SP_N into the left half of the complex ω plane.

Finally, for $\theta' > \theta_1$ application of Olver's theorem [32] at the two first-order near saddle-point locations yields the following general expression for the generalized Brillouin precursor:

$$A_B(z,t) = \frac{1}{2\pi} \mathrm{Re} \left[i \left[2 \exp \left\{ \frac{z}{c} \phi(\omega_{\mathrm{SP}_N^+}, \theta') \right\} \left[\frac{\pi c}{z} \right]^{1/2} a_0(\omega_{\mathrm{SP}_N^+}) [1 + O(z^{-1})] + 2 \exp \left\{ \frac{z}{c} \phi(\omega_{\mathrm{SP}_N^-}, \theta') \right\} \left[\frac{\pi c}{z} \right]^{1/2} a_0(\omega_{\mathrm{SP}_N^-}) [1 + O(z^{-1})] \right] \right] \tag{2.13}$$

as $z \to +\infty$ uniformly for $\theta' \geq \theta_1 + \Delta$ for positive Δ that is arbitrarily small. In Eq. (2.13), $\omega_{SP_N^{\pm}}(\theta') = \pm\Psi(\theta') - i[2\delta\zeta(\theta')]/3$ denotes the locations of the near saddle points in the right and left half of the complex ω plane, and the coefficients $a_0(\omega_{SP_N^{\pm}})$ are given by the expression

$$a_0(\omega_{SP_N^{\pm}}) = \frac{\tilde{U}(\omega_{SP_N^{\pm}} - \omega_c)}{2\left[-\frac{1}{2}\frac{d^2}{d\omega^2}[\phi(\omega_{SP_N^{\pm}}, \theta')]\right]^{1/2}} . \quad (2.14)$$

The proper values of the argument of the term appearing inside the square root in the denominator of Eq. (2.14) are $-\pi/2$ (for the right near saddle point $\omega_{SP_N^{+}}$) and $+\pi/2$ (for the left near saddle point $\omega_{SP_N^{-}}$).

Upon substitution of the analytic expressions found by Oughstun [4] and Oughstun and Sherman [5,6] for the near saddle-point locations as well as for the derivatives of the phase function at them as a function of θ' in Eqs. (2.8), (2.11), and (2.13), the approximate expressions of the nonuniform asymptotic behavior of the generalized Brillouin precursor field for an input unit amplitude, ultrashort Gaussian-modulated harmonic signal presented in Ref. [29] are obtained. Notice that as the parameter θ' approaches the value θ_1 where the order of the near saddle points changes discontinuously, Olver's method [32] fails and a uniform asymptotic analysis has to be performed. This uniform expansion is described in the next section.

III. UNIFORM ASYMPTOTIC DESCRIPTION OF THE PROPAGATED FIELD

For Gaussian-pulse propagation the general expression for the asymptotic approximation of the integral representation of the propagated field is found to be given in a continuous manner by Eq. (2.4). When the uniform asymptotic theory is invoked the resulting expressions for $A_S(z,t)$ and $A_B(z,t)$ are uniformly valid for all $\theta' \geq 1$ and hence the general expression in Eq. (2.4) is also uniformly valid for all $\theta' \geq 1$. For most values of θ', only one of the terms $A_S(z,t)$ or $A_B(z,t)$ appearing in Eq. (2.4) is important at a time. There is a short interval of θ' around the value [4,5] $\theta_{SB} \cong \theta_0 - (4\delta^2 b^2/3\theta_0\omega_0^4)$ when the relevant upper near and two distant saddle points have equal dominance, so that both terms in Eq. (2.4) are significant for fixed values of the propagation distance z. This θ' range is the transition period in which the presence of both terms in Eq. (2.4) leads to a continuous transition in the behavior of the propagated field, as was shown in Appendix D of Ref. [6].

In this section the discontinuities associated with the nonuniform asymptotic method of Olver around the space-time points $\theta' = 1$ and $\theta' = \theta_1$ are removed through use of uniform asymptotic expressions for the generalized Sommerfeld and Brillouin precursor fields, which are derived here for the case of an input unit amplitude, ultrashort Gaussian-modulated harmonic signal.

A. Generalized Sommerfeld precursor

The uniform asymptotic expansion resulting from two first-order saddle points $\omega_{\pm}(\theta)$ with equal imaginary parts and with real parts that approach $\pm\infty$, respectively, as θ approaches some critical value θ_{cr_S} was developed by Handelsman and Bleistein [33]. In their application of this asymptotic expansion, Oughstun and co-workers [4,6,9] obtained a uniformly valid approximation of the Sommerfeld or first precursor field for all $\theta \geq \theta_{cr_S} = 1$.

The general uniform asymptotic description of the Sommerfeld precursor field is given by [4,6]

$$A_S(z,t) = \mathrm{Re}\left\{\exp\left[-i\frac{z\beta(\theta)}{c}\right][2\alpha(\theta)\exp\{-i\pi/2\}]^{\nu} \times \left[\gamma_0 J_{\nu}\left[\frac{z\alpha(\theta)}{c}\right] + 2\alpha(\theta)\exp\{-i\pi/2\}\gamma_1 J_{\nu+1}\left[\frac{z\alpha(\theta)}{c}\right]\right]\right\} + R_1(z,\theta) \quad (3.1)$$

as $z \to +\infty$, uniformly for all $\theta \geq 1$. Here $J_{\nu}(\zeta)$ is the Bessel function of the first kind of order ν. The real parameter $\nu > 0$ is determined from the expression

$$\tilde{u}(\omega) = \omega^{-(1+\nu)}\tilde{q}(\omega) \quad (3.2)$$

for large $|\omega|$, with $\tilde{u}(\omega)$ being the spectral function appearing in Eq. (1.9), and where $\tilde{q}(\omega)$ has a Laurent series expansion that is convergent for large $|\omega|$ and is such that

$$\lim_{|\omega| \to +\infty}[\tilde{q}(\omega)] = \lim_{|\omega| \to +\infty}[\omega^{1+\nu}\tilde{u}(\omega)] \neq 0 . \quad (3.3)$$

When $\nu < 0$ the uniform asymptotic description provided by Eq. (3.1) may still be applicable provided that its limiting value as θ tends to unity from above is finite [33]. The remainder term $R_1(z,\theta)$ appearing in Eq. (3.1) is found to satisfy the inequality (with K a positive real constant independent of both θ and z)

$$|R_1(z,\theta)| \leq K\frac{|2\alpha(\theta)|^{\nu+1}}{z}\left\{\left|J_{\nu+1}\left[\frac{z\alpha(\theta)}{c}\right]\right| + \left|J_{\nu+2}\left[\frac{z\alpha(\theta)}{c}\right]\right|\right\} \quad (3.4)$$

for $z \geq Z > 0$ and $\theta \rightarrow 1^+$, and is small for large z independent of $\alpha(\theta)$.

For the case of Gaussian-pulse propagation the spectral function of interest is given as

$$\tilde{u}(\omega)=\tilde{q}(\omega)=\exp\{i(\omega t_0+\psi)\}\tilde{U}(\omega-\omega_c) \tag{3.5}$$

in Eq. (3.2), where $\tilde{U}(\omega-\omega_c)$ is given by Eq. (1.13), so that the corresponding real parameter ν is found to be

$$\nu=-1 \ . \tag{3.6}$$

The coefficients appearing in Eq. (3.1) are given by

$$\alpha(\theta')=\frac{i}{2}[\phi(\omega_{\mathrm{SP}_D^+},\theta')-\phi(\omega_{\mathrm{SP}_D^-},\theta')] \tag{3.7a}$$

$$\cong\xi(\theta')\left\{(\theta'-1)+\frac{b^2}{2\{\xi^2(\theta')+\delta^2[1-\eta(\theta')]^2\}}\right\}, \tag{3.7b}$$

$$\beta(\theta')=\frac{i}{2}[\phi(\omega_{\mathrm{SP}_D^+},\theta')+\phi(\omega_{\mathrm{SP}_D^-},\theta')] \tag{3.8a}$$

$$\cong -i\delta\left\{[1+\eta(\theta')](\theta'-1)+\frac{b^2[1-\eta(\theta')]}{2\{\xi^2(\theta')+\delta^2[1-\eta(\theta')]^2\}}\right\}, \tag{3.8b}$$

$$\gamma_0(\theta')=\frac{1}{2}\left\{\tilde{U}(\omega_{\mathrm{SP}_D^+}-\omega_c)\left[\frac{1}{2\alpha(\theta')}\right]^{1+\nu}\left[\frac{4\alpha^3(\theta')}{i\phi^{(2)}(\omega_{\mathrm{SP}_D^+},\theta')}\right]^{1/2}+\tilde{U}(\omega_{\mathrm{SP}_D^-}-\omega_c)\left[\frac{-1}{2\alpha(\theta')}\right]^{1+\nu}\left[\frac{-4\alpha^3(\theta')}{i\phi^{(2)}(\omega_{\mathrm{SP}_D^-},\theta')}\right]^{1/2}\right\}$$

$$\cong\frac{\xi^{1/2}(\theta')}{b}\left\{\xi(\theta')\left[(\theta'-1)+\frac{b^2}{2\{\xi^2(\theta')+\delta^2[1-\eta(\theta')]^2\}}\right]\right\}^{3/2} \tag{3.9a}$$

$$\times\left\{\tilde{U}(\omega_{\mathrm{SP}_D^+}-\omega_c)\left[\xi(\theta')+i\frac{3\delta}{2}[1-\eta(\theta')]\right]+\tilde{U}(\omega_{\mathrm{SP}_D^-}-\omega_c)\left[\xi(\theta')-i\frac{3\delta}{2}[1-\eta(\theta')]\right]\right\}, \tag{3.9b}$$

$$\gamma_1(\theta')=\frac{1}{4\alpha(\theta')}\left\{\tilde{U}(\omega_{\mathrm{SP}_D^+}-\omega_c)\left[\frac{1}{2\alpha(\theta')}\right]^{1+\nu}\left[\frac{4\alpha^3(\theta')}{i\phi^{(2)}(\omega_{\mathrm{SP}_D^+},\theta')}\right]^{1/2}\right.$$

$$\left.-\tilde{U}(\omega_{\mathrm{SP}_D^-}-\omega_c)\left[\frac{-1}{2\alpha(\theta')}\right]^{1+\nu}\left[\frac{-4\alpha^3(\theta')}{i\phi^{(2)}(\omega_{\mathrm{SP}_D^-},\theta')}\right]^{1/2}\right\} \tag{3.10a}$$

$$\cong\frac{\xi^{1/2}(\theta')}{2b}\left\{\xi(\theta')\left[(\theta'-1)+\frac{b^2}{2\{\xi^2(\theta')+\delta^2[1-\eta(\theta')]^2\}}\right]\right\}^{1/2}$$

$$\times\left\{\tilde{U}(\omega_{\mathrm{SP}_D^+}-\omega_c)\left[\xi(\theta')+i\frac{3\delta}{2}[1-\eta(\theta')]\right]-\tilde{U}(\omega_{\mathrm{SP}_D^-}-\omega_c)\left[\xi(\theta')-i\frac{3\delta}{2}[1-\eta(\theta')]\right]\right\}. \tag{3.10b}$$

Substitution of these expressions into Eq. (3.1) then yields the uniform asymptotic approximation of the generalized Sommerfeld precursor as

$$A_S(z,t)\sim\frac{\xi(\theta')}{2b}\left[(\theta'-1)+\frac{b^2}{2\{\xi^2(\theta')+\delta^2[1-\eta(\theta')]^2\}}\right]^{1/2}$$

$$\times\exp\left\{\frac{-\delta z}{c}\left[[1+\eta(\theta')](\theta'-1)+\frac{b^2[1-\eta(\theta')]}{2\{\xi^2(\theta')+\delta^2[1-\eta(\theta')]^2\}}\right]\right\}$$

$$\times\mathrm{Re}\left\{i(\tilde{U}(\omega_{\mathrm{SP}_D^+}-\omega_c)\{\xi(\theta')+i\tfrac{3}{2}\delta[1-\eta(\theta')]\}+\tilde{U}(\omega_{\mathrm{SP}_D^-}-\omega_c)\{\xi(\theta')-i\tfrac{3}{2}\delta[1-\eta(\theta')]\})\right.$$

$$\times J_{-1}\left[\frac{z}{c}\xi(\theta')\left[(\theta'-1)+\frac{b^2}{2\{\xi^2(\theta')+\delta^2[1-\eta(\theta')]^2\}}\right]\right]$$

$$+(\tilde{U}(\omega_{\mathrm{SP}_D^+}-\omega_c)\{\xi(\theta')+i\tfrac{3}{2}\delta[1-\eta(\theta')]\}-\tilde{U}(\omega_{\mathrm{SP}_D^-}-\omega_c)\{\xi(\theta')-i\tfrac{3}{2}\delta[1-\eta(\theta')]\})$$

$$\left.\times J_0\left[\frac{z}{c}\xi(\theta')\left[(\theta'-1)+\frac{b^2}{2\{\xi^2(\theta')+\delta^2[1-\eta(\theta')]^2\}}\right]\right]\right\} \tag{3.11}$$

as $z \to +\infty$ uniformly for all $\theta' \geq 1$. In Eqs. (3.7b), (3.8b), (3.9b), (3.10b), and (3.11) use was made of the approximate analytic expressions [4–6] of the right ($\omega_{SP_D^+}$) and left ($\omega_{SP_D^-}$) distant saddle-point locations and of the derivatives of the phase function $\phi(\omega,\theta')$ at them.

Since $\nu < 0$, the uniform asymptotic approximation given in Eq. (3.11) is valid for all $\theta' \geq 1$ only if its limit as θ' tends to unity from above is finite. In this limit the functions $\xi(\theta')$ and $\eta(\theta')$ attain the limiting forms

$$\lim_{\theta' \to 1^+} [\xi(\theta')] = \frac{b}{[2(\theta'-1)]^{1/2}} , \tag{3.12a}$$

$$\lim_{\theta' \to 1^+} [\eta(\theta')] = 1 , \tag{3.12b}$$

so that the argument of the Bessel functions appearing in Eq. (3.11) reduces to Brillouin's first-order approximation [2–5]

$$\lim_{\theta' \to 1^+} \left[\frac{z}{c} \xi(\theta') \left[(\theta'-1) + \frac{b^2}{2\{\xi^2(\theta') + \delta^2[1-\eta(\theta')]^2\}} \right] \right] = \frac{z}{c} b [2(\theta'-1)]^{1/2} . \tag{3.13}$$

Consequently, for values of θ' very close to unity the argument of the Bessel functions is very small so that the small argument limiting form of the Bessel functions [35] appearing in Eq. (3.11) may be employed with the result

$$\lim_{\theta' \to 1^+} [A_S(z,t)] \sim \tfrac{1}{2} \exp\left\{ -2\frac{\delta z}{c}(\theta'-1) \right\} \operatorname{Re}\left\{ -i\frac{b^2 z}{2c} [\tilde{U}(\omega_{SP_D^+} - \omega_c) + \tilde{U}(\omega_{SP_D^-} - \omega_c)] + \frac{b}{[2(\theta'-1)]^{1/2}} [\tilde{U}(\omega_{SP_D^+} - \omega_c) - \tilde{U}(\omega_{SP_D^-} - \omega_c)] \right\} . \tag{3.14}$$

As θ' tends to unity from above the distant saddle points tend to the limiting locations $\pm\infty - i2\delta$ and the values of the spectral functions $\tilde{U}(\omega_{SP_D^\pm} - \omega_c)$ given in Eq. (1.13) become

$$\lim_{\theta' \to 1^+} [\tilde{U}(\omega_{SP_D^\pm} - \omega_c)] = 0 , \tag{3.15}$$

so that the limit in Eq. (3.14) becomes

$$\lim_{\theta' \to 1^+} [A_S(z,t)] = 0 , \tag{3.16}$$

which is finite. The fact that the generalized Sommerfeld precursor field vanishes for $\theta' = 1$ is not consistent with our numerical results. This inconsistency is due to the nonvanishing width $2T > 0$ of the initial Gaussian-pulse envelope at $z = 0$ and disappears in the limit as $2T \to 0$, in which case one obtains a δ-function pulse. As a consequence, the expression given in Eq. (3.11) constitutes the appropriate approximation of the uniform asymptotic description of the generalized Sommerfeld precursor field for all $\theta' > 1$, which is due to an input unit amplitude, ultrashort Gaussian-modulated harmonic field.

B. Generalized Brillouin precursor

The uniform asymptotic expansion for two neighboring first-order saddle points $\omega_1(\theta)$ and $\omega_2(\theta)$ that coalesce into a single second-order saddle point ω_s as θ approaches some critical value θ_{cr_B} was developed by Chester, Friedman, and Ursell [34]. In their application of this uniform asymptotic theory Oughstun and co-workers [4,6,9] derived an asymptotic approximation of the Brillouin or second precursor field that is uniformly valid for all $\theta \geq 1$.

For the particular case of Gaussian-pulse propagation that is of central interest here, this work is directly applicable for all $\theta' \geq 1$. It is still necessary to treat the two cases $1 \leq \theta' \leq \theta_1$ and $\theta' \geq \theta_1$ separately because the approximate analytic expressions [4] for the locations of the near saddle points differ in the two cases. Nonetheless, the results for the two cases combined are continuous at $\theta' = \theta_1$ and constitute an asymptotic approximation of the second precursor field $A_B(z,t)$ due to a unit amplitude, ultrashort Gaussian-modulated harmonic signal, that is uniformly valid for all $\theta' \geq 1$.

The uniform asymptotic description of the generalized Brillouin precursor field as $z \to +\infty$, for all values of θ' in the domain $1 \leq \theta' \leq \theta_1$, is then given by

$$A_B(z,t) \sim \exp\left\{ \frac{z}{c}\alpha_0(\theta') \right\} \left\{ \frac{1}{2} \left[\frac{c}{z} \right]^{1/3} \operatorname{Re}\{ i[\tilde{U}(\omega_{SP_1} - \omega_c)|h_1(\theta')| + \tilde{U}(\omega_{SP_2} - \omega_c)|h_2(\theta')|] \} \operatorname{Ai}\left[|\alpha_1(\theta')| \left[\frac{z}{c} \right]^{2/3} \right] - \frac{1}{2|\alpha_1(\theta')|^{1/2}} \left[\frac{c}{z} \right]^{2/3} \operatorname{Re}\{ i[\tilde{U}(\omega_{SP_1} - \omega_c)|h_1(\theta')| - \tilde{U}(\omega_{SP_2} - \omega_c)|h_2(\theta')|] \} \times \operatorname{Ai}^{(1)}\left[|\alpha_1(\theta')| \left[\frac{z}{c} \right]^{2/3} \right] \right\} , \tag{3.17}$$

where $\operatorname{Ai}(J)$ and $\operatorname{Ai}^{(1)}(J)$ denote [31], respectively, the Airy function and its first derivative and where the remainder

term is $O(1/z)$. The coefficients appearing in Eq. (3.17) are given by

$$\alpha_0(\theta')=\tfrac{1}{2}[\phi(\omega_{\mathrm{SP}_1},\theta')+\phi(\omega_{\mathrm{SP}_2},\theta')] \tag{3.18a}$$

$$\cong\frac{-2\delta\zeta(\theta')}{3}(\theta'-\theta_0)-\frac{\delta b^2}{\theta_0\omega_0^4}\left[|\Psi(\theta')|^2[\alpha\zeta(\theta')-1]+\frac{4\delta^2\zeta^2(\theta')}{9}\left[\frac{\alpha\zeta(\theta')}{3}-1\right]\right], \tag{3.18b}$$

$$\alpha_1^{1/2}(\theta')=\{\tfrac{3}{4}[\phi(\omega_{\mathrm{SP}_1},\theta')-\phi(\omega_{\mathrm{SP}_2},\theta')]\}^{1/3} \tag{3.19a}$$

$$\cong\left\{|\Psi(\theta')|\left[\tfrac{3}{2}(\theta'-\theta_0)+\frac{b^2}{\theta_0\omega_0^4}[\tfrac{3}{4}\alpha|\Psi(\theta')|^2+\alpha\delta^2\zeta^2(\theta')-2\delta^2\zeta(\theta')]\right]\right\}^{1/3}, \tag{3.19b}$$

$$h_{1,2}(\theta')=\left[\frac{2\alpha_1^{1/2}(\theta')}{\phi^{(2)}(\omega_{\mathrm{SP}_{1,2}},\theta')}\right]^{1/2} \tag{3.20a}$$

$$\cong\left\{\left[\frac{2\theta_0\omega_0^4}{b^2(3\alpha|\Psi(\theta')|\pm2\delta[1-\alpha\zeta(\theta')])}\right]^3\right.$$
$$\left.\times|\Psi(\theta')|\left[\tfrac{3}{2}(\theta'-\theta_0)+\frac{b^2}{\theta_0\omega_0^4}[\tfrac{3}{4}\alpha|\Psi(\theta')|^2+\alpha\delta^2\zeta^2(\theta')-2\delta^2\zeta(\theta')]\right]\right\}^{1/6}, \tag{3.20b}$$

for values of θ' in the range $1\le\theta'\le\theta_1$, where the upper sign corresponds to $h_1(\theta')$ and the lower sign corresponds to $h_2(\theta')$ in Eqs. (3.20a) and (3.20b). In Eqs. (3.17)–(3.20) use was made of the approximate analytic expressions [4–6] of the upper (ω_{SP_1}) and lower (ω_{SP_2}) near saddle-point locations given in Sec. II B (viz., $\omega_{\mathrm{SP}_{1,2}}(\theta')=i[\pm|\Psi(\theta')|-2\delta\zeta(\theta')/3]$, when $1\le\theta'\le\theta_1$).

In the limit as θ' approaches the critical value θ_1 from below Eq. (3.17) reduces to

$$\lim_{\theta'\to\theta_1^-}[A_B(z,t)]=A_B(z,t_1)$$
$$\sim\frac{\omega_0}{2\pi3^{1/2}}\Gamma(\tfrac{1}{3})\left[\frac{2\theta_0\omega_0 c}{\alpha b^2 z}\right]^{1/3}\mathrm{Re}\{i\tilde{U}(\omega_{\mathrm{SP}_N}-\omega_c)\}\exp\left\{\frac{2\delta z}{3\alpha c}\left[(\theta_0-\theta_1)+\frac{4\delta^2b^2}{9\alpha\theta_0\omega_0^4}\right]\right\}, \tag{3.21}$$

as $z\to+\infty$ for $\theta'=\theta_1=(ct_1/z)$ when the two first-order near saddle points have coalesced into a single second-order saddle point at $\omega_{\mathrm{SP}_N}\cong-i(2\delta/3\alpha)$.

Finally, the uniform asymptotic description of the generalized Brillouin precursor field as $z\to+\infty$, for values of θ' in the domain $\theta'\ge\theta_1$, is given by

$$A_B(z,t)\sim\exp\left\{\frac{z}{c}\alpha_0(\theta')\right\}\left\{\frac{1}{2}\left[\frac{c}{z}\right]^{1/3}\mathrm{Re}\{i[\tilde{U}(\omega_{\mathrm{SP}_N^+}-\omega_c)|h^+(\theta')|+\tilde{U}(\omega_{\mathrm{SP}_N^-}-\omega_c)|h^-(\theta')|]\}\times\mathrm{Ai}\left[-|\alpha_1(\theta')|\left[\frac{z}{c}\right]^{2/3}\right]\right.$$
$$+\frac{1}{2|\alpha_1(\theta')|^{1/2}}\left[\frac{c}{z}\right]^{2/3}\mathrm{Re}\{[\tilde{U}(\omega_{\mathrm{SP}_N^+}-\omega_c)|h^+(\theta')|-\tilde{U}(\omega_{\mathrm{SP}_N^-}-\omega_c)|h^-(\theta')|]\}$$
$$\left.\times\mathrm{Ai}^{(1)}\left[-|\alpha_1(\theta')|\left[\frac{z}{c}\right]^{2/3}\right]\right\}, \tag{3.22}$$

where the remainder term is $O(1/z)$. The coefficients appearing in Eq. (3.22) are given by

$$\alpha_0(\theta')=\tfrac{1}{2}[\phi(\omega_{\mathrm{SP}_N^+},\theta')+\phi(\omega_{\mathrm{SP}_N^-},\theta')] \tag{3.23a}$$

$$\cong\frac{-2\delta\zeta(\theta')}{3}(\theta'-\theta_0)-\frac{\delta b^2}{\theta_0\omega_0^4}\left[[1-\alpha\zeta(\theta')]\Psi^2(\theta')+\frac{4\delta^2\zeta^2(\theta')}{9}\left[\frac{\alpha\zeta(\theta')}{3}-1\right]\right], \tag{3.23b}$$

$$\alpha_1^{1/2}(\theta')=\{\tfrac{3}{4}[\phi(\omega_{\mathrm{SP}_N^+},\theta')-\phi(\omega_{\mathrm{SP}_N^-},\theta')]\}^{1/3} \tag{3.24a}$$

$$\cong\left\{-i\tfrac{3}{2}\Psi(\theta')\left[(\theta'-\theta_0)-\frac{b^2}{2\theta_0\omega_0^4}\{\tfrac{4}{3}\delta^2\zeta(\theta')[2-\alpha\zeta(\theta')]+\alpha\Psi^2(\theta')\}\right]\right\}^{1/3}, \tag{3.24b}$$

and

$$h^{\pm}(\theta')=\left[\frac{\mp 2\alpha_1^{1/2}(\theta')}{\phi^{(2)}(\omega_{\mathrm{SP}_N^{\pm}},\theta')}\right]^{1/2} \tag{3.25a}$$

$$\cong\left\{\left[i\frac{2\theta_0\omega_0^4}{3\alpha b^2\Psi(\theta')}\right]^3\left[\frac{-i3\Psi(\theta')}{2}\right]\left[(\theta'-\theta_0)-\frac{b^2}{2\theta_0\omega_0^4}\{\tfrac{4}{3}\delta^2\zeta(\theta')[2-\alpha\zeta(\theta')]+\alpha\Psi^2(\theta')\}\right]\right\}^{1/6}, \tag{3.25b}$$

for all θ' in the range $\theta'\geq\theta_1$. In Eqs. (3.22)–(3.25) use was made of the approximate analytic expressions [4–6] for the right ($\omega_{\mathrm{SP}_N^+}$) and left ($\omega_{\mathrm{SP}_N^-}$) near saddle-point locations given in Sec. II B (viz., $\omega_{\mathrm{SP}_N^{\pm}}(\theta')=\pm\Psi(\theta')-i[2\delta\zeta(\theta')/3]$, when $\theta'\geq\theta_1$). Notice that as θ' approaches the critical value θ_1 from above, Eq. (3.22) reduces to the limiting expression (3.21).

Taken together, Eqs. (3.17) and (3.22) constitute the uniform asymptotic expression of the generalized Brillouin precursor for an input unit amplitude, ultrashort Gaussian-modulated harmonic signal for all $\theta'\geq 1$ and reduce to the nonuniform asymptotic expressions given in Sec. II when θ' is bounded away from θ_1.

IV. DISCUSSION

The numerical evaluation of the integral representation given in Eq. (1.12) describing the propagation of an input unit amplitude, ultrashort Gaussian-modulated harmonic signal in a Lorentz medium that is based upon Hosono's Laplace-transform method [30] (referred to here as the Hosono code) constitutes the first numerical experiment that is used as a comparison with our asymptotic description. A second, independent method of numerically evaluating this same integral representation is based on the numerical implementation of the method of steepest descents [31], and is referred to here as the asymptotic code. The results of this code constitute the second numerical experiment and are used as a second independent verification of our theoretical results. The agreement between the results of these two numerical experiments for each of the cases we have considered, a sample of which appears in this section, is remarkably exceptional and provides a secure measure of the accuracy in the description of ultrashort Gaussian-pulse propagation that is afforded by both the nonuniform and uniform theories.

When the modern asymptotic method of Olver [32] is used to evaluate the integral representation in Eq. (1.12), along with approximate analytic expressions for the saddle-point locations and the derivatives of the phase function at them, as determined by Oughstun [4], the approximate expressions appearing in Ref. [29] for the generalized Sommerfeld precursor $A_S(z,t)$ and the generalized Brillouin precursor $A_B(z,t)$ are obtained. The results of a numerical implementation of these expressions is depicted here for comparison and is referred to as the analytical nonuniform theory. Its predictions of the generalized Sommerfeld precursor field amplitudes are found to be greater than the respective results of the two numerical experiments for this precursor field, while its predictions of the generalized Brillouin precursor fields are of approximately the same amplitude but are found to oscillate at higher frequencies than the respective ones predicted by the two numerical experiments.

The primary source of these discrepancies is found to be from the use of the approximate analytic expressions for the saddle-point locations, and, to a lesser extent, from the use of the approximate analytic expressions for the derivatives of the phase function at the saddle-point locations. Even though these approximate expressions have been found [5–9] to be of sufficient accuracy when used to describe the propagation of either an input δ-function pulse, an input unit-step-function modulated harmonic signal, or a rectangular-function modulated harmonic signal of arbitrary initial pulse width in either a single- or double-resonance Lorentz medium, such is not the case here because of the exponential behavior of the Gaussian envelope. Indeed, a close examination of the general expression (1.13) for the Gaussian spectral amplitude appearing in Eq. (1.12) reveals that any deviation of the analytically determined approximate saddle-point locations from the exact locations (which can only be determined with sufficient accuracy using numerical techniques) affects the results exponentially, especially for broad initial pulses. This should then be the primary source of the observed differences between the predictions of the analytical nonuniform theory and the results of the two numerical experiments. It is further expected that, to a smaller degree, the analytically determined approximate expressions for the derivatives of the phase function at the saddle-point locations that are used in the implementation of Olver's asymptotic method will further aggravate these discrepancies.

In order to verify our assertions as well as to improve the asymptotic description of ultrashort Gaussian-pulse propagation in a Lorentz medium, a numerical evaluation (referred to here as the numerical nonuniform theory) of the general expressions (2.5) and (2.6) for the generalized Sommerfeld precursor field, and (2.8), (2.9), and (2.11)–(2.14) for the generalized Brillouin precursor field, has been performed. In this implementation of the asymptotic method of Olver, the exact, numerically determined saddle-point locations and exact expressions for the derivatives of the phase function were used. As expected, the results are found to be in excellent agreement with the results of the two numerical experiments, thus proving the validity of the asymptotic description of the propagation of the input unit amplitude, ultrashort Gaussian-modulated harmonic signal in a Lorentz medium. The tradeoff for the increased accuracy in the description of the propagated field is the use of more gen-

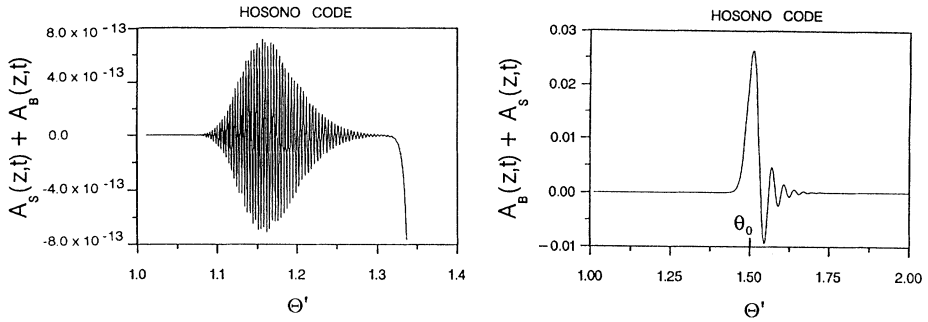

FIG. 3. The dynamical field evolution due to an input Gaussian-modulated cosine field with initial pulse width $2T = 0.2$ fsec and a carrier frequency $\omega_c = 3.1416 \times 10^{16}$ sec^{-1} at a propagation distance $z = 112.47 z_d$, where z_d is the absorption depth at the carrier frequency ω_c. The experimental results of the Hosono code are shown in the top two diagrams while the respective experimental results of the asymptotic code are shown in the bottom two diagrams.

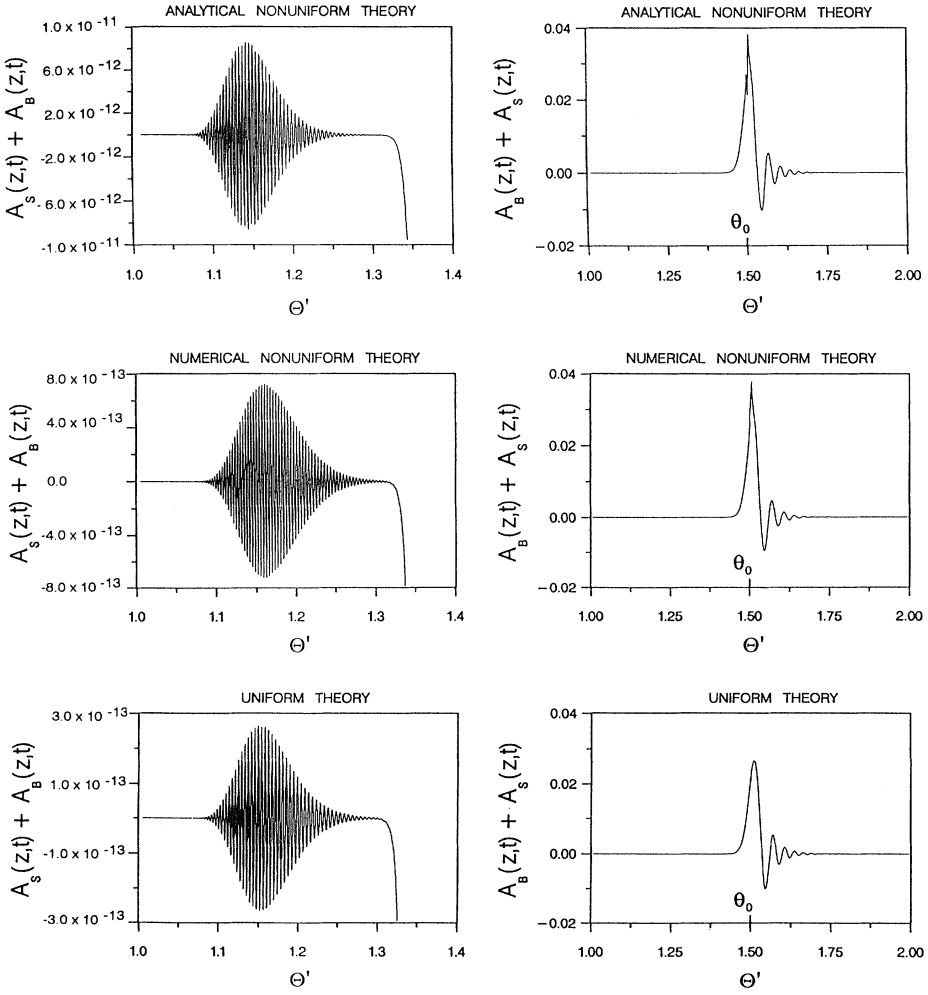

FIG. 4. The dynamical field evolution due to an input Gaussian-modulated cosine field with initial pulse width $2T = 0.2$ fsec and a carrier frequency $\omega_c = 3.1416 \times 10^{16}$ sec^{-1} at a propagation distance $z = 112.47 z_d$, where z_d is the absorption depth at the carrier frequency ω_c. The results of the analytical nonuniform theory are shown in the top two diagrams, the respective results of the numerical nonuniform theory are shown in the middle two diagrams, and the respective uniform theory results are shown in the bottom two diagrams.

eral expressions that, although entirely correct, depend more on numerical techniques. Nevertheless, since the sources of the discrepancies between the nonuniform theory and the experiments have now been identified, we can still cautiously use the analytic approximate expressions for the saddle-point locations and the derivatives of the phase function at them in Olver's method, to get the only available, though in some cases rough, analytical description of ultrashort Gaussian-pulse propagation in a Lorentz medium.

The results of both the analytical and numerical nonuniform theories are nonuniform when θ' tends to unity from above and when θ' approaches θ_I. In order to overcome these two difficulties the uniform asymptotic theory is used. Its numerical implementation (referred to here as the uniform theory) using the derived expressions (3.11) for the generalized Sommerfeld precursor field and (3.17) and (3.22) for the generalized Brillouin precursor field is uniformly valid for all $\theta' \geq 1$. The exact, numerically determined saddle-point locations are used here only to evaluate the Gaussian spectral amplitude functions $\tilde{U}(\omega_{SP_D^{\pm}} - \omega_c)$, $\tilde{U}(\omega_{SP_{1,2}} - \omega_c)$, and $\tilde{U}(\omega_{SP_N^{\pm}} - \omega_c)$ appearing in Eqs. (3.11), (3.17), and (3.22), respectively, since use of analytic approximate expressions can seriously degrade the performance of the uniform asymptotic method. On the other hand, in order to have expressions that are more tractable analytically than the respective expressions used for the numerical nonuniform theory, the approximate, analytically determined expressions for the saddle-point locations and the derivatives of the phase function at them were used everywhere else in the uniform asymptotic description. It is then expected that the uniform theory will improve the description afforded both by the analytical nonuniform theory and the numerical nonuniform theory when θ' tends to unity from above and when θ' tends to θ_1, but that it will not agree with the two numerical experiments as well as the numerical nonuniform theory.

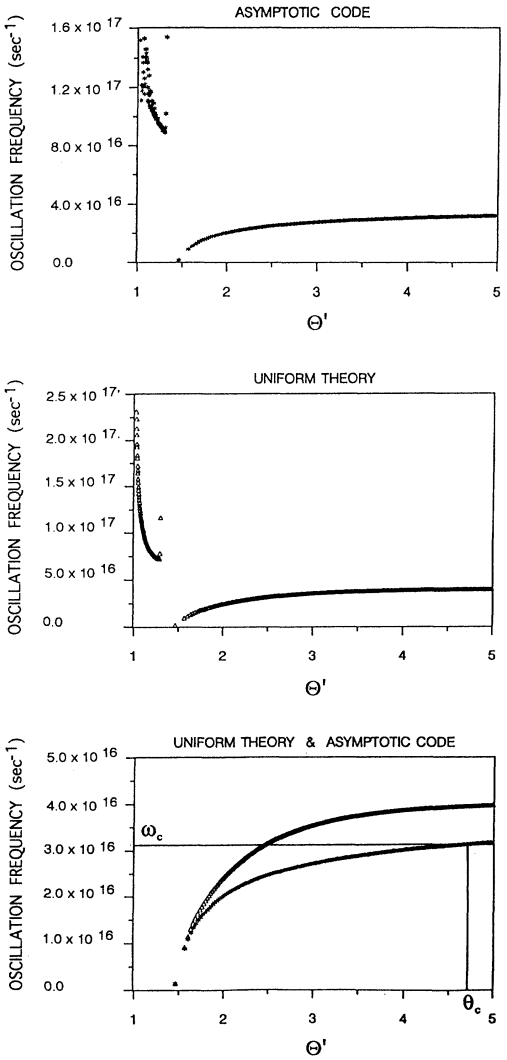

FIG. 5. Evolution of the instantaneous angular frequency of oscillation for the dynamical field evolution due to an input Gaussian-modulated cosine field with initial pulse width $2T=0.2$ fsec and a carrier frequency $\omega_c = 3.1416 \times 10^{16}$ sec^{-1} at a propagation distance $z = 112.47 z_d$, where z_d is the absorption depth at the carrier frequency ω_c. The asterisks in the top and bottom diagrams denote the frequency of oscillation values that were determined from the asymptotic code, while the triangles in the middle and bottom diagrams denote the frequency of oscillation values that were determined from the uniform theory.

Attention is now turned to the results of the two numerical experiments and their comparison with both the nonuniform and uniform asymptotic theories. Brillouin's choice of the medium parameters are used throughout this numerical comparison. The case of an input unit amplitude, Gaussian-modulated cosine field is depicted in Figs. 3–5 when the initial pulse width is $2T=0.2$ fsec, with carrier frequency $\omega_c = 3.1416 \times 10^{16}$/sec, which is below the absorption band of the medium. This set of the input field parameters corresponds to one oscillation of the harmonic signal under the full width at e^{-1} maximum points of the Gaussian envelope at $z=0$. The propagation distance $z=5.0$ μm is equal to 112.47 absorption lengths z_d at the signal frequency ω_c. The total propagated field $A(z,t) = A_S(z,t) + A_B(z,t)$ calculated using the Hosono code is depicted at the top of Fig. 3 and is seen to be dominated by the generalized Sommerfeld precursor field for $1 < \theta' < \theta_{SB}$, while it is dominated by the generalized Brillouin precursor field for $\theta' > \theta_{SB}$ where $\theta_{SB} \cong 1.334$. Since the input carrier frequency ω_c is below the medium absorption band, the peak amplitude of the generalized Brillouin precursor field is many orders of magnitude greater than the peak amplitude of the generalized Sommerfeld precursor field. The corresponding results of the total propagated field calculated using the asymptotic code are depicted at the bottom of Fig. 3. Comparison of the respective wave forms in Fig. 3 shows that the two independent numerical experiments describing the propagated field are in complete agreement. The analytical predictions of the total propagated field due to the same input field considered in Fig. 3, calculated using the analytical nonuniform theory, the numerical nonuniform theory and the uniform theory, respectively, are depicted in Fig. 4. The observed discrepancies between the

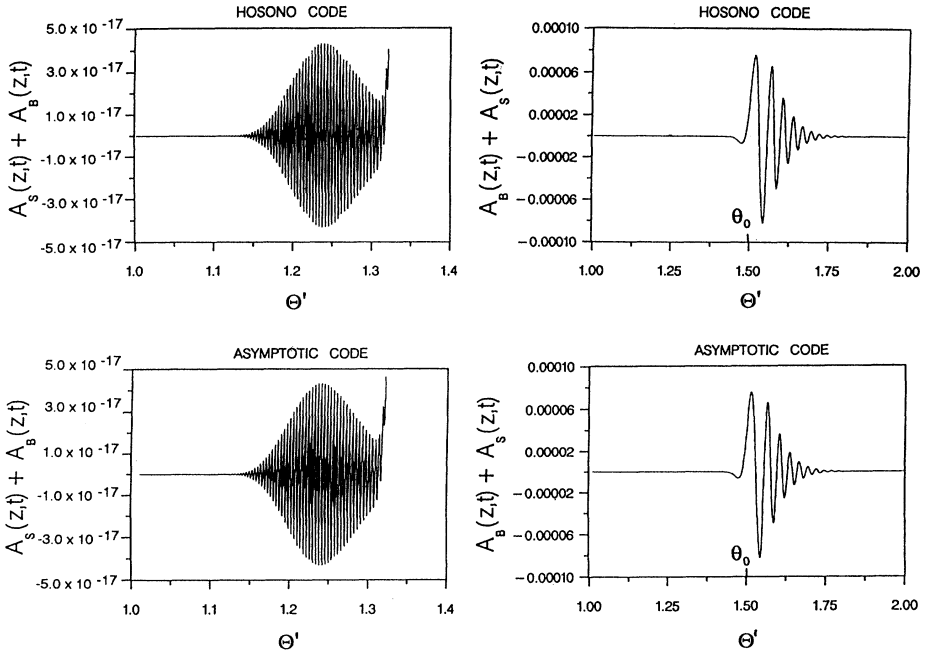

FIG. 6. The dynamical field evolution due to an input Gaussian-modulated cosine field with initial pulse width $2T = 0.314$ fsec and a carrier frequency $\omega_c = 4.0 \times 10^{16}$ sec^{-1} at a propagation distance $z = 1332.97 z_d$, where z_d is the absorption depth at the carrier frequency ω_c. The experimental results of the Hosono code are shown in the top two diagrams while the respective experimental results of the asymptotic code are shown in the bottom two diagrams.

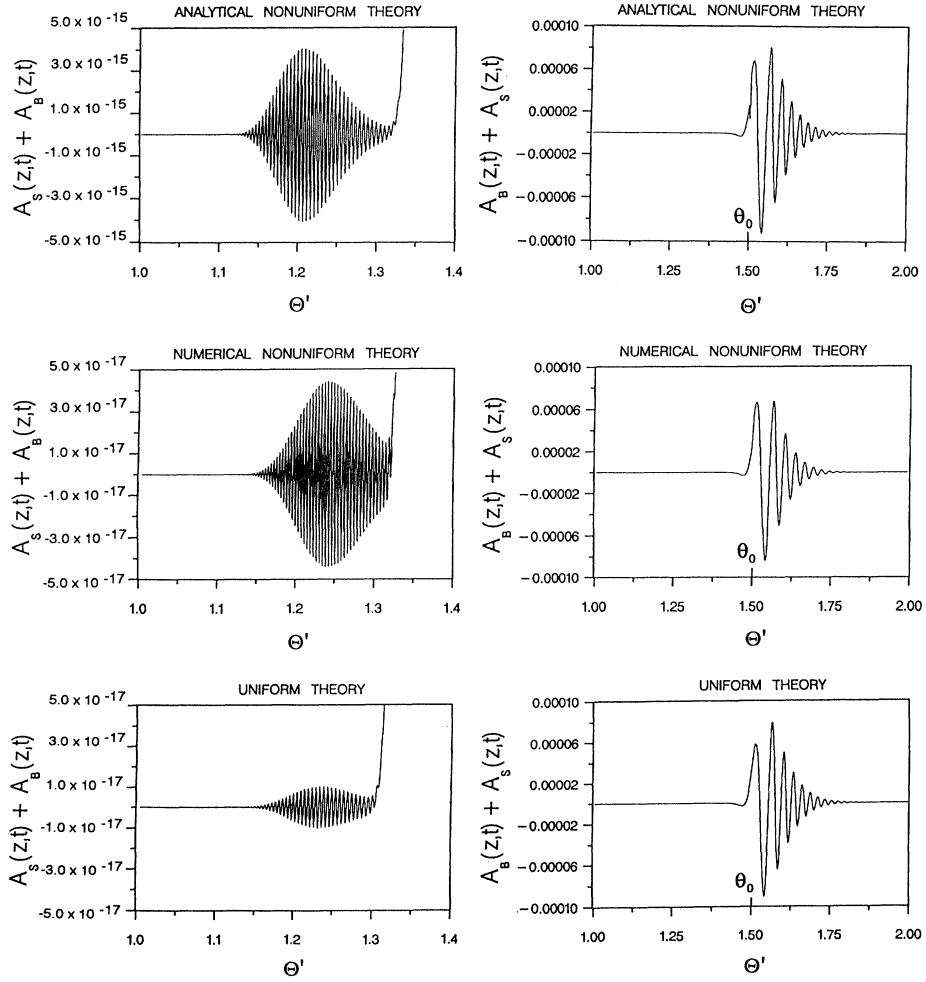

FIG. 7. The dynamical field evolution due to an input Gaussian-modulated cosine field with initial pulse width $2T = 0.314$ fsec and a carrier frequency $\omega_c = 4.0 \times 10^{16}$ sec^{-1} at a propagation distance $z = 1332.97 z_d$, where z_d is the absorption depth at the carrier frequency ω_c. The results of the analytical nonuniform theory are shown in the top two diagrams, the respective result of the numerical nonuniform theory are shown in the middle two diagrams, and the respective uniform theory results are shown in the bottom two diagrams.

analytical nonuniform theory and the two numerical experiments are due to the use of the approximate analytic expressions for the saddle-point locations and the derivatives of the phase function at them. When exact, numerically determined saddle-point locations and exact expressions for the derivatives of the phase function at them are used, the results of the numerical nonuniform theory are found to be in excellent agreement with the two numerical experiments for all θ' except for the two small θ' neighborhoods about the space-time points $\theta'=1$ and $\theta'=\theta_1$ when the nonuniform asymptotic theory breaks down. The results of the uniform asymptotic theory, presented at the bottom of Fig. 4, overcome this difficulty and are uniformly valid for all $\theta' \geq 1$. It is to be remembered that several approximations have been introduced in the uniform asymptotic description so that the resultant expressions are more tractable analytically. Hence, as expected, the uniform asymptotic description does not completely agree with the two numerical experiments as well as does the numerical nonuniform theory, but it clearly describes the propagated field structure better than the analytical nonuniform theory.

The numerically determined instantaneous frequencies of oscillation for this propagated field are depicted in Fig. 5. In the upper diagram the asterisks mark the oscillation frequency values determined from the asymptotic code, while in the middle diagram the triangles mark the oscillation frequency values determined from the uniform theory. A comparison of these two results for the oscillation frequency of the generalized Brillouin precursor is presented in the bottom diagram of the figure, where again the asterisks and triangles denote frequencies of oscillation evaluated numerically from the asymptotic code and the uniform asymptotic theory, respectively. The observed difference between the two results is due primarily to the inaccuracy inherent in the analytic description of the near saddle-point locations.

Similar degrees of accuracy are obtained when the input carrier frequency of the pulse is increased through and above the medium absorption band that is defined over the real frequency range $(\omega_0^2-\delta^2)^{1/2} \leq \omega_c \leq (\omega_1^2-\delta^2)^{1/2}$. Figures 6–8 depict the results when

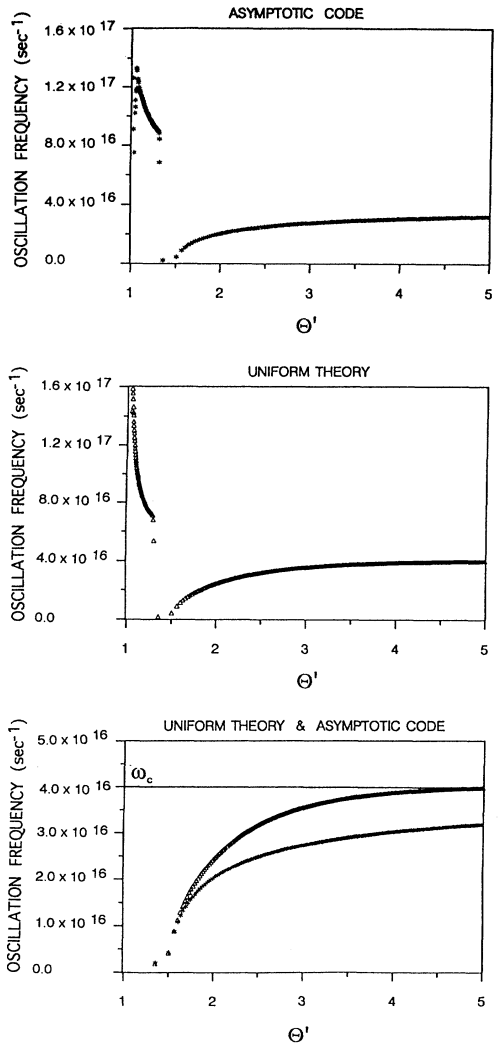

FIG. 8. Evolution of the instantaneous angular frequency of oscillation for the dynamical field evolution due to an input Gaussian-modulated cosine field with initial pulse width $2T=0.314$ fsec and a carrier frequency $\omega_c=4.0\times10^6$ sec^{-1} at a propagation distance $z=1332.97z_d$, where z_d is the absorption depth at the carrier frequency ω_c. The asterisks in the top and bottom diagrams denote the frequency of oscillation values that were determined from the asymptotic code, while the triangles in the middle and bottom diagrams denote the frequency of oscillation values that were determined from the uniform theory.

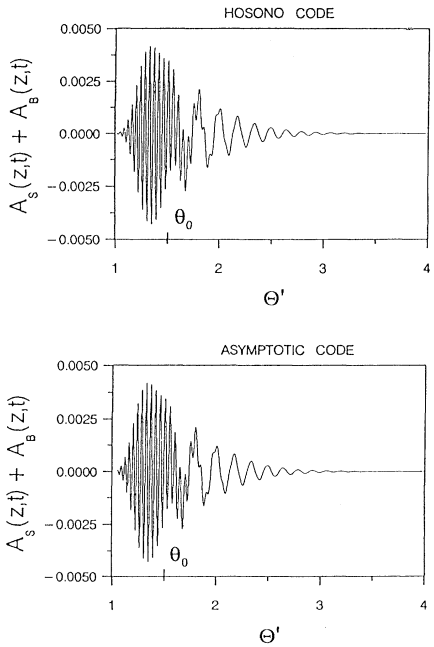

FIG. 9. The dynamical field evolution due to an input Gaussian-modulated cosine field with initial pulse width $2T=0.2$ fsec and a carrier frequency $\omega_c=5.75\times10^{16}$ sec^{-1} at a propagation distance $z=41.96z_d$, where z_d is the absorption depth at the carrier frequency ω_c. The experimental result of the Hosono code is shown in the top diagram while the respective experimental result of the asymptotic code is shown in the bottom diagram.

$\omega_c = \omega_0$, the undamped resonance frequency of the medium, which is near the lower end of the absorption band. Figures 9–11 depict the results when $\omega_c = 5.75 \times 10^{16}$/sec, which is near the upper end of the absorption band, while Figs. 12–14 depict the results when $\omega_c = 10.0 \times 10^{16}$/sec, which is well above the upper end of the absorption band. These results clearly show the accuracy that the asymptotic description possesses over the entire frequency range $\omega_c \in [0, \infty)$. Again, the only major inaccuracy in the analytic theory arises from the approximations made in describing the saddle-point dynamics analytically [5]; this inaccuracy is clearly removed by using numerically determined saddle-point locations.

The observed structure of the dynamical field evolution depicted in Figs. 3–14 is easily understood from the asymptotic representation

$$A(z,t) \sim A_S(z,t) + A_B(z,t) \tag{4.1}$$

as $z \to +\infty$ for all $\theta' \geq 1$ in a single-resonance Lorentz medium. Because of the initial Gaussian envelope spectrum (1.13), the asymptotic description of $A_S(z,t)$ and $A_B(z,t)$ each contain a Gaussian factor of the form $\exp\{-(T^2/4)[\mathrm{Re}(\omega_{\mathrm{SP}}) - \omega_c]^2\}$, where ω_{SP} denotes the distant saddle-point location in the right half of the complex ω plane for the generalized Sommerfeld precursor $A_S(z,t)$, while ω_{SP} denotes the relevant near saddle-point location for the generalized Brillouin precursor $A_B(z,t)$. The asymptotic description of each generalized precursor field also contains an exponential attenuation factor that is given by the product of the propagation distance z with the attenuation that is characteristic of the real phase behavior at the relevant saddle point. Finally, the instantaneous oscillation frequency of each precursor field in the mature dispersion regime is approximately given by $\mathrm{Re}\{\omega_{\mathrm{SP}}(\theta')\}$ for an ultrashort pulse.

In particular, the instantaneous frequency of the oscillation of the generalized Sommerfeld precursor is obtained from the derivative of the oscillatory phase term in the uniform asymptotic expansion (3.11) as

$$\begin{aligned}\omega_S(\theta') = \xi(\theta') &+ \frac{b^2\theta'}{2\xi(\theta')(\theta'^2-1)^2}\left[\frac{b^2\{\xi^2(\theta') - 5\delta^2(1-\eta(\theta'))^2\}}{\{\xi^2(\theta') + \delta^2(1-\eta(\theta'))^2\}^2} - 2(\theta'-1)\right] \\ &- \frac{9\delta c b^2 \theta'(1-\eta(\theta'))}{2z\xi^3(\theta')(\theta'^2-1)^2}\left[1 + \frac{9\delta^2(1-\eta(\theta'))^2}{\xi^2(\theta')}\right]^{-1} \\ &+ \frac{T^2}{2}\frac{\delta b^2 c}{z}\frac{\theta'}{\xi^2(\theta')(\theta'^2-1)^2}[\xi(\theta')(3-\eta(\theta')) + 2\omega_c(\eta(\theta')-1)] \,. \end{aligned} \tag{4.2}$$

The first term on the right-hand side of this expression is just the real part of the distant saddle-point location $\omega_{\mathrm{SP}_D^+}(\theta') = \xi(\theta') - i\delta(1+\eta(\theta'))$, where $\xi(\theta')$ monotonically decreases from infinity at $\theta' = 1$ and approaches $(\omega_1^2 - \delta^2)^{1/2}$ as $\theta' \to +\infty$. The first three terms on the right-hand side of this expression give the instantaneous oscillation frequency of the Sommerfeld precursor field for the δ-function pulse [4–6], where, to a good approximation, $\omega_S \cong \xi(\theta') \cong \omega_E$. Here $\omega_E \geq (\omega_1^2 - \delta^2)^{1/2}$ is the real frequency solution [12] of $v_E(\omega_E) = c/\theta'$, with $v_E(\omega)$ being the monochromatic energy transport velocity [14] for a single-resonance Lorentz medium, given by

$$v_E(\omega) = \frac{c}{n_r(\omega) + \dfrac{\omega n_i(\omega)}{\delta}} \,, \tag{4.3}$$

where $n_r(\omega)$ and $n_i(\omega)$ are the real and imaginary parts, respectively, of the complex index of refraction (1.5). With this substitution the instantaneous frequency of oscillation of the generalized Sommerfeld precursor becomes

$$\begin{aligned}\omega_S(\theta') \cong \omega_E(\theta') &+ \frac{T^2}{2}\frac{\delta b^2 c}{z}\frac{\theta'}{\xi^2(\theta')(\theta'^2-1)^2} \\ &\times [\xi(\theta')(3-\eta(\theta')) + 2\omega_c(\eta(\theta')-1)]\end{aligned} \tag{4.4}$$

in the mature-dispersion regime.

Since $\eta(\theta')$ monotonically decreases from 1 to 0 as θ' increases from 1 to infinity, the second term on the right-hand side in Eq. (4.4) is non-negative for all $\theta' \geq 1$. Hence, the instantaneous oscillation frequency of the generalized Sommerfeld precursor due to an input ultrashort Gaussian pulse is increased above that for an input δ-function pulse and approaches it as $z \to +\infty$. Hence, $\omega_S \geq (\omega_1^2 - \delta^2)^{1/2}$ for all parameters of an input ultrashort Gaussian pulse. If the input carrier frequency ω_c is chosen to be above the medium absorption band so that $\omega_c > (\omega_1^2 - \delta^2)^{1/2}$, then the instantaneous oscillation frequency of the generalized Sommerfeld precursor will chirp downwards across ω_c at a sufficiently large, fixed propagation distance z. In that particular case, let θ_E denote the value of θ' at which $\omega_E = \omega_c$; this space-time point corresponds to that point in the field which travels at the velocity $v_E(\omega_c) = c/\theta_E$ given by the energy transport velocity of a monochromatic plane-wave field with frequency ω_c [12]. Let θ_c denote the value of θ' at which $\omega_S = \omega_c$; this space-time point corresponds to that point in the generalized Sommerfeld precursor field evolution when the instantaneous frequency of oscillation crosses the value $\omega_c > (\omega_1^2 - \delta^2)^{1/2}$. It is then seen from Eq. (4.4) that $\theta_c = \theta_E$ when $T = 0$ (i.e., in the limit as the initial

Gaussian pulse approaches a δ-function pulse). Furthermore, θ_c is increased above θ_E when $T>0$ and approaches θ_E with a z^{-1} dependence as the propagation distance increases.

In a similar fashion, the instantaneous frequency of oscillation of the generalized Brillouin precursor is obtained from the derivative of the oscillatory phase term in the uniform asymptotic expansion (3.22) as

$$\omega_B(\theta')\cong\omega_E(\theta')-\frac{T^2}{3}\frac{\delta b^2 c}{\Psi(\theta')\omega_0^2 z}\frac{\theta'}{\left\{\theta'^2-\theta_0^2+\frac{3\alpha b^2}{\omega_0^2}\right\}^2}\left[\Psi(\theta')[\Psi(\theta')-\omega_c](3\alpha-2)+\zeta(\theta')\left[3\alpha\omega_0^2-\frac{4\delta^2\zeta(\theta')(3\alpha-2)}{3}\right]\right] \tag{4.5}$$

for $\theta'\geq\theta_1$ when $\omega_c\leq(\omega_0^2-\delta^2)^{1/2}$. Since $\Psi(\theta')\leq(\omega_0^2-\delta^2)^{1/2}$ for all $\theta'\geq\theta_1$, then the quantity appearing in the square brackets in the above expression is nonnegative for all $\theta'\geq\theta_1$ when $\omega_c\leq(\omega_0^2-\delta^2)^{1/2}$. Hence, the instantaneous oscillation frequency of the oscillatory portion of the generalized Brillouin precursor due to an input ultrashort Gaussian pulse is decreased below that for an input δ-function pulse and approaches it as $z\to+\infty$.

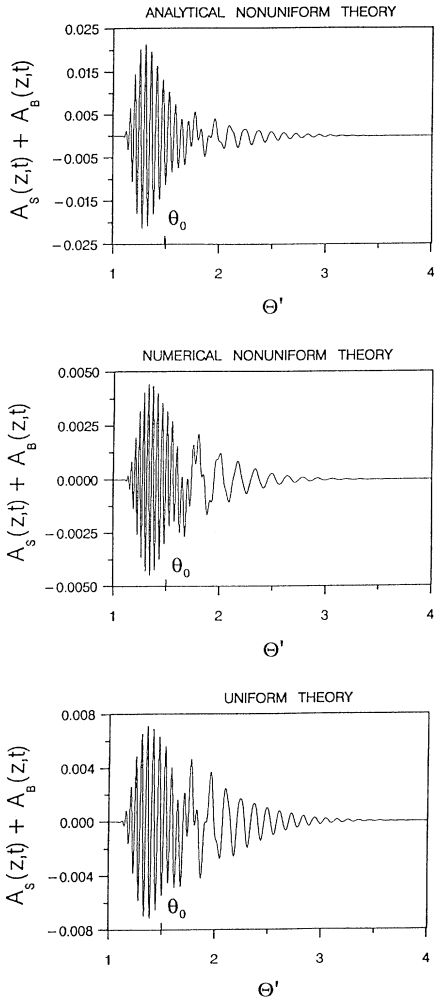

FIG. 10. The dynamical field evolution due to an input Gaussian-modulated cosine field with initial pulse width $2T=0.2$ fsec and a carrier frequency $\omega_c=5.75\times10^{16}$ sec^{-1} at a propagation distance $z=41.96z_d$, where z_d is the absorption depth at the carrier frequency ω_c. The result of the analytical nonuniform theory is shown in the top diagram, the respective result of the numerical nonuniform theory is shown in the middle diagram, and the respective uniform theory result is shown in the bottom diagram.

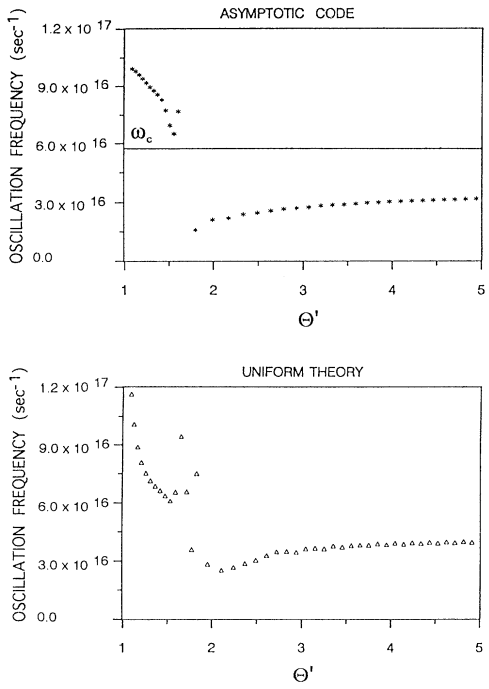

FIG. 11. Evolution of the instantaneous angular frequency of oscillation for the dynamical field evolution due to an input Gaussian-modulated cosine field with initial pulse width $2T=0.2$ fsec and a carrier frequency $\omega_c=5.75\times10^{16}$ sec^{-1} at a propagation distance $z=41.96z_d$, where z_d is the absorption depth at the carrier frequency ω_c. The asterisks in the top diagram denote the frequency of oscillation values that were determined from the asymptotic code, while the triangles in the bottom diagram denote the frequency of oscillation values that were determined from the uniform theory.

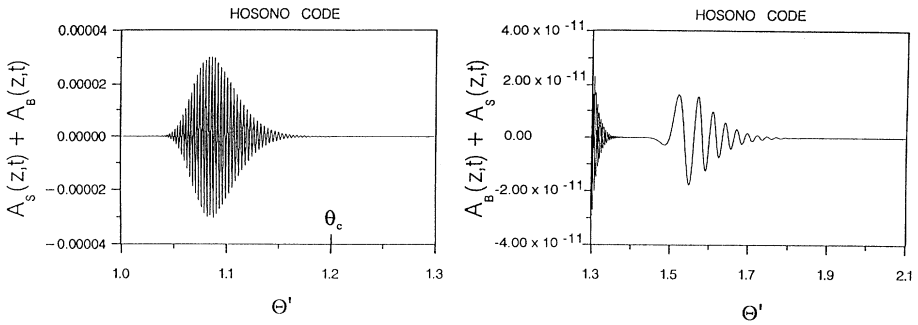

FIG. 12. The dynamical field evolution due to an input Gaussian-modulated cosine field with initial pulse width $2T=0.2$ fsec and a carrier frequency $\omega_c=10.0\times10^{16}$ sec^{-1} at a propagation distance $z=15.09z_d$, where z_d is the absorption depth at the carrier frequency ω_c. The experimental results of the Hosono code are shown in the top two diagrams while the respective experimental results of the asymptotic code are shown in the bottom two diagrams.

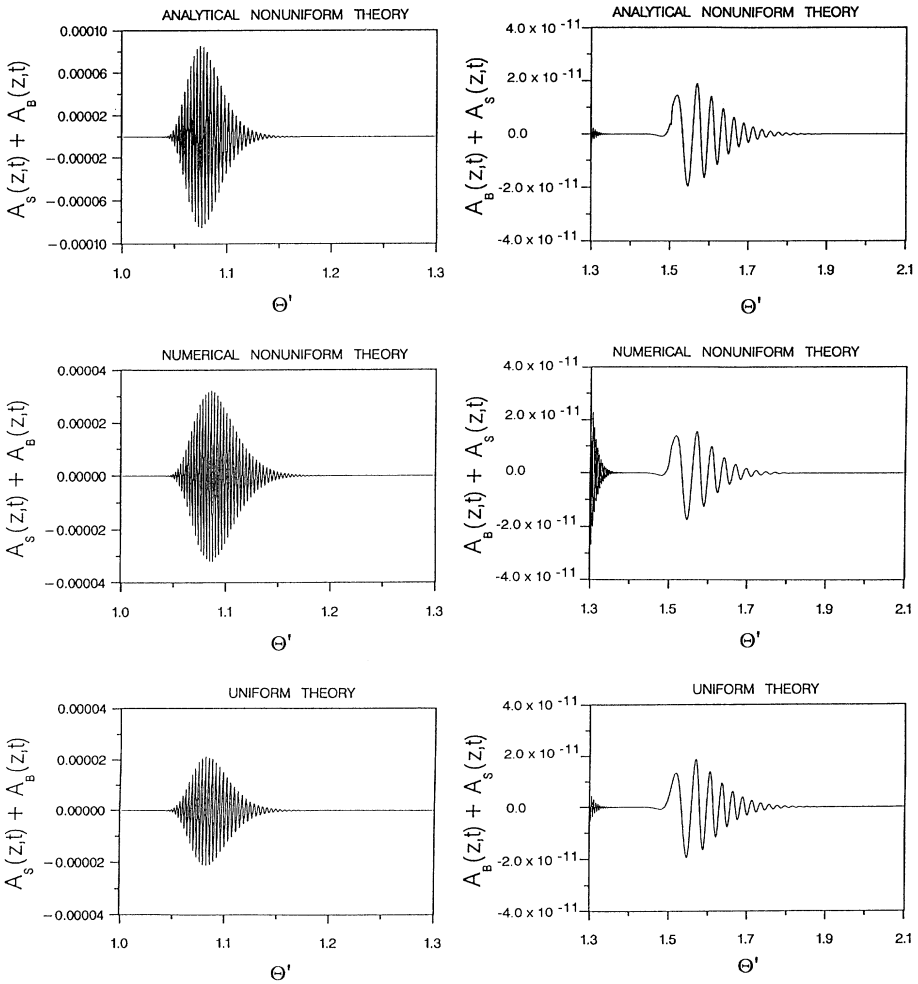

FIG. 13. The dynamical field evolution due to an input Gaussian-modulated cosine field with initial pulse width $2T=0.2$ fsec and a carrier frequency $\omega_c=10.0\times10^{16}$ sec^{-1} at a propagation distance $z=15.09z_d$, where z_d is the absorption depth at the carrier frequency ω_c. The results of the analytical nonuniform theory are shown in the top two diagrams, the respective results of the numerical nonuniform theory are shown in the middle two diagrams, and the respective uniform theory results are shown in the bottom two diagrams.

Hence $\omega_B \leq (\omega_0^2-\delta^2)^{1/2}$ for all parameters of an input ultrashort Gaussian pulse with $\omega_c \leq (\omega_0^2-\delta^2)^{1/2}$. The instantaneous oscillation frequency of the generalized Brillouin precursor will then chirp upwards across ω_c at a sufficiently large fixed propagation distance z. In this case, let θ_E denote the value of θ' at which $\omega_E=\omega_c$ and let θ_c denote the value of θ' at which $\omega_B=\omega_c$. The space-time point θ_c then corresponds to that point in the generalized Brillouin precursor field evolution when the instantaneous frequency of oscillation crosses the value $\omega_c \leq \omega_0$. It is then seen from Eq. (4.5) that $\theta_c=\theta_E$ when $T=0$ (i.e., in the limit as the input Gaussian pulse approaches a δ-function pulse). Furthermore, θ_c is increased above θ_E when $T>0$ and approaches θ_E with a z^{-1} dependence as the propagation distance increases.

When the input carrier frequency ω_c lies in the absorption band of the medium, so that $(\omega_0^2-\delta^2)^{1/2} < \omega_c < (\omega_1^2-\delta^2)^{1/2}$, then $\omega_S(\theta')$, as given by Eq. (4.4) with $\omega_E(\theta')$ now replaced by $\xi(\theta')$, is bounded below by $(\omega_1^2-\delta^2)^{1/2}$. However, $\omega_B(\theta')$, as given by Eq. (4.5) with $\omega_E(\theta')$ now replaced by $\Psi(\theta')$, is no longer bounded above by $(\omega_0^2-\delta^2)^{1/2}$ since the quantity appearing in the large square brackets in that expression may now become negative for some value $\theta'>\theta_1$ and remain so for all larger values of θ'. The maximum frequency attained by $\omega_B(\theta')$ is then increased above $(\omega_0^2-\delta^2)^{1/2}$ by a factor that increases as the square of the initial pulse width and decreases as z^{-1}. Notice, however, that this behavior has been obtained here for the case of ultrashort pulses whose initial pulse rise time is either less than or on the order of $1/\delta$. Nevertheless, these results clearly show that the instantaneous oscillation frequency of the generalized Brillouin precursor can enter the absorption band of the medium when the input carrier frequency ω_c is in the absorption band, provided that the observation distance z is not too large. As z increases, the propagated field characteristics approach that due to an input δ-function pulse [29].

For $0 \leq \omega_c < (\omega_0^2-\delta^2)^{1/2}$ the generalized Brillouin precursor field $A_B(z,t)$ dominates the entire propagated field

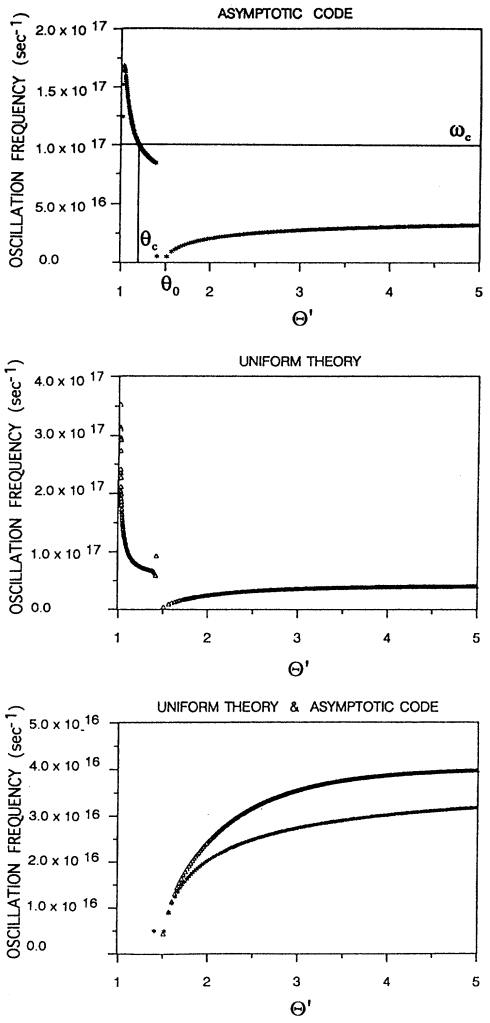

FIG. 14. Evolution of the instantaneous angular frequency of oscillation for the dynamical field evolution due to an input Gaussian-modulated cosine field with initial pulse width $2T=0.2$ fsec and a carrier frequency $\omega_c=10.0\times10^{16}$ sec^{-1} at a propagation distance $z=15.09z_d$, where z_d is the absorption depth at the carrier frequency ω_c. The asterisks in the top and bottom diagrams denote the frequency of oscillation values that were determined from the asymptotic code, while the triangles in the middle and bottom diagrams denote the frequency of oscillation values that were determined from the uniform theory.

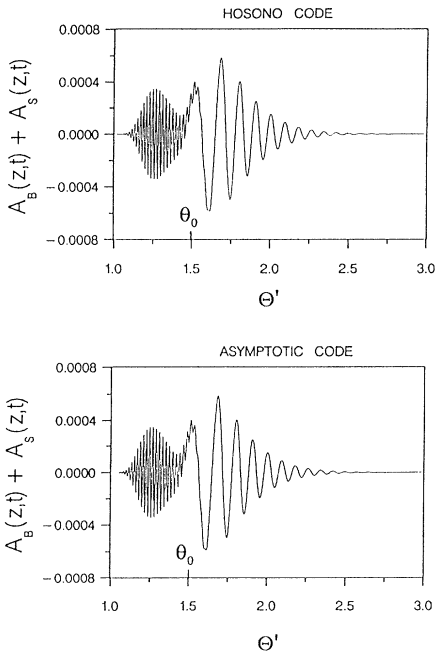

FIG. 15. The dynamical field evolution due to an input Gaussian-modulated cosine field with initial pulse width $2T=0.2$ fsec and a carrier frequency $\omega_c=5.75\times10^{16}$ sec^{-1} at a propagation distance $z=83.92z_d$, where z_d is the absorption depth at the carrier frequency ω_c. The experimental result of the Hosono code is shown in the top diagram while the respective experimental result of the asymptotic code is shown in the bottom diagram.

evolution, as illustrated in Fig. 3 for an input Gaussian-modulated cosine field with initial pulse width $2T=2.0\times10^{-16}$ sec and carrier frequency $\omega_c=3.1416\times10^{16}$/sec at a fixed propagation distance $z=112.47z_d$ in the Lorentz-type medium under consideration. The value $\theta_c\cong4.679\,66$ in Fig. 5 indicates the point in the field evolution at which the instantaneous oscillation frequency equals ω_c; for $\theta'<\theta_c$ the instantaneous oscillation frequency of $A_B(z,t)$ is less than ω_c, while for $\theta'>\theta_c$ it is greater than ω_c. It is about this point that the Gaussian factor $\exp\{-(T^2/4)[\mathrm{Re}(\omega_{\mathrm{SP}_N^+})-\omega_c]^2\}$ peaks to its maximum value. However, because the attenuation of the Brillouin precursor identically vanishes at $\theta'=\theta_0=n(0)$ while it monotonically increases for all $|\theta'-\theta_0|>0$, the peak in the propagated field is shifted toward this earlier space-time point. As the propagation distance increases, the location of the peak amplitude in the propagated field approaches the space-time point $ct/z=\theta_0$ from above for an input Gaussian-modulated cosine wave as considered here; for an input Gaussian-modulated sine wave [29] the initial field has a zero at the peak in the initial envelope so that the location of the peak amplitude in the propagated field just follows the space-time point $ct/z=\theta_0$. Notice that the Sommerfeld precursor is virtually absent from the total propagated-field structure, as the initial spectrum in this case is practically zero in the region of the distant saddle points. Indeed, the peak amplitude in the Sommerfeld precursor at this propagation distance is reduced by $\sim10^{-11}$ from the peak amplitude of the Brillouin precursor. As the initial pulse width $2T$ is decreased from the value considered here the spectrum broadens and, for the cosine-wave case, the Sommerfeld precursor becomes more apparent as the total propagated-field structure approaches that for an input δ-function pulse [4–6]; for the sine-wave case the field vanishes as $T\to0$. On the other hand, as the initial pulse width $2T$ is increased the spectrum narrows and the peak in the Gaussian factor begins to dom-

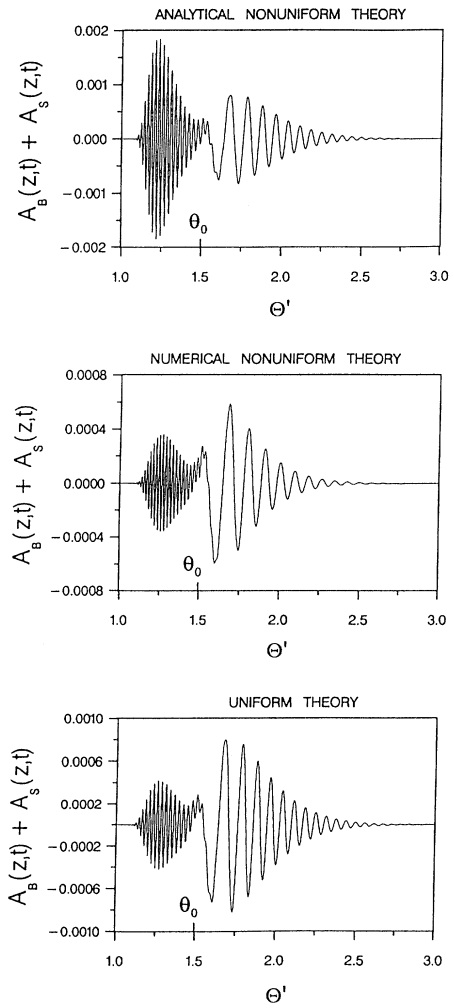

FIG. 16. The dynamical field evolution due to an input Gaussian-modulated cosine field with initial pulse width $2T=0.2$ fsec and a carrier frequency $\omega_c=5.75\times10^{16}$ sec^{-1} at a propagation distance $z=83.92z_d$, where z_d is the absorption depth at the carrier frequency ω_c. The result of the analytical nonuniform theory is shown in the top diagram, the respective result of the numerical nonuniform theory is shown in the middle diagram, and the respective uniform theory result is shown in the bottom diagram.

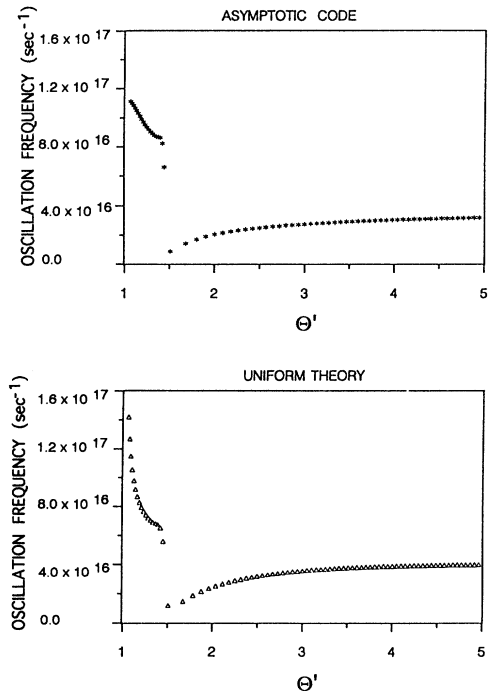

FIG. 17. Evolution of the instantaneous angular frequency of oscillation for the dynamical field evolution due to an input Gaussian-modulated cosine field with initial pulse width $2T=0.2$ fsec and a carrier frequency $\omega_c=5.75\times10^{16}$ sec^{-1} at a propagation distance $z=83.92z_d$, where z_d is the absorption depth at the carrier frequency ω_c. The asterisks in the top diagram denote the frequency of oscillation values that were determined from the asymptotic code, while the triangles in the bottom diagram denote the frequency of oscillation values that were determined from the uniform theory.

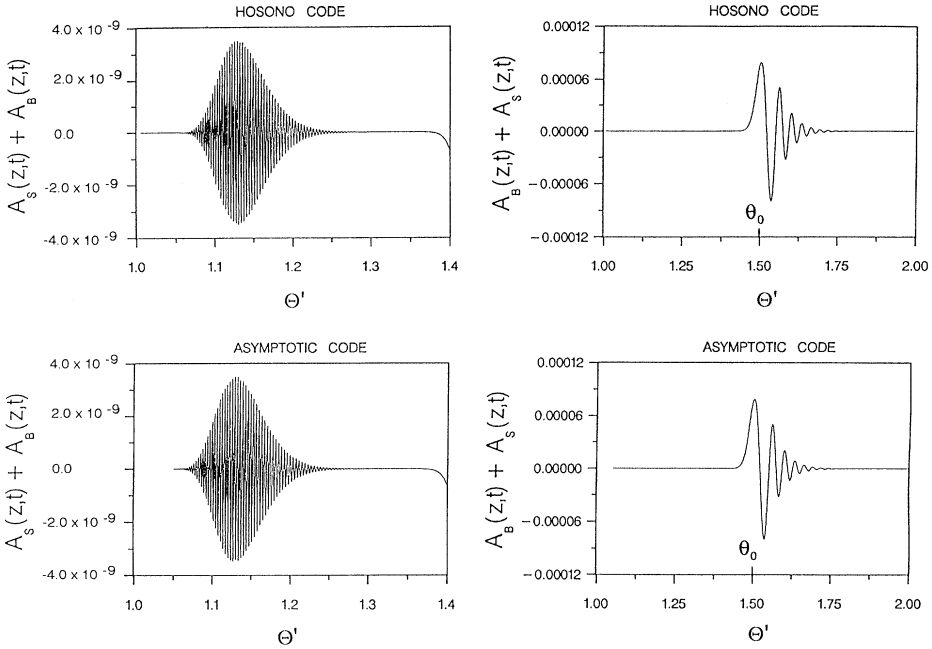

FIG. 18. The dynamical field evolution due to an input Gaussian-modulated cosine field with initial pulse width $2T=0.2$ fsec and a carrier frequency $\omega_c=5.75\times10^{16}$ sec^{-1} at a propagation distance $z=419.60z_d$, where z_d is the absorption depth at the carrier frequency ω_c. The experimental results of the Hosono code are shown in the top two diagrams, while the respective experimental results of the asymptotic code are shown in the bottom two diagrams.

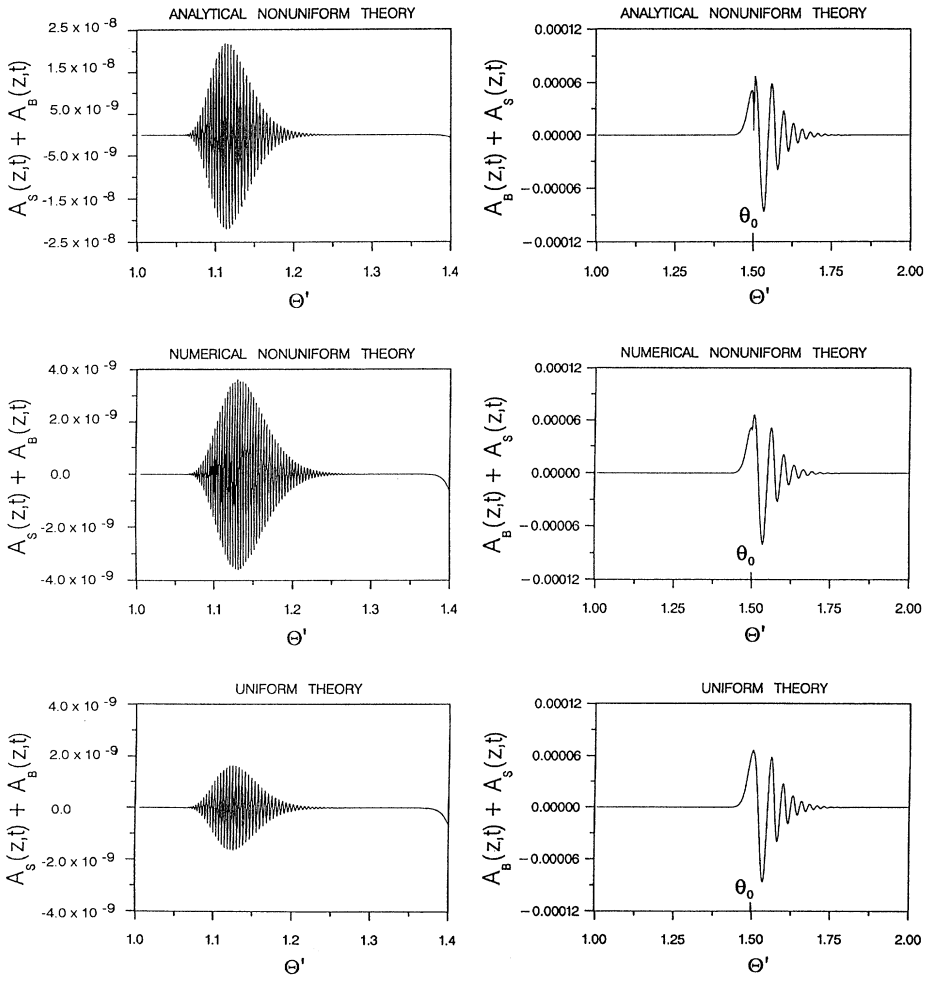

FIG. 19. The dynamical field evolution due to an input Gaussian- modulated cosine field with initial pulse width $2T=0.2$ fsec and a carrier frequency $\omega_c=5.75\times10^{16}$ sec^{-1} at a propagation distance $z=419.60z_d$, where z_d is the absorption depth at the carrier frequency ω_c. The results of the analytical nonuniform theory are shown in the top two diagrams, the respective results of the numerical nonuniform theory are shown in the middle two diagrams, and the respective uniform theory results are shown in the bottom two diagrams.

inate the total field evolution $A(z,t) \sim A_B(z,t)$ as the spectral amplitude at $\theta' = \theta_0$ (the zero attenuation point in the Brillouin precursor) decreases. Nevertheless, as the propagation distance is increased (i.e., as the dispersion becomes more mature), the attenuation will cause the peak amplitude to shift towards $\theta' = \theta_0$. As the initial pulse width is increased well above $1/\delta$, the total field $A(z,t) \sim A_B(z,t)$ is dominated by the Gaussian factor in the Brillouin precursor as the spectral amplitude is practically zero everywhere except in a small neighborhood of ω_c. In that case, it is more appropriate to expand the integral representation about ω_c rather than about the dominant saddle point. In the ultrashort $T \leq 1/\delta$ case, the point in the field evolution at which the oscillation frequency passes through ω_c is given by the value $\theta_c \cong \theta_E$, so that the signal velocity of an ultrashort Gaussian pulse is (approximately) the same as that obtained for the unit-step-function modulated signal for $0 \leq \omega_c \leq \omega_0$ and is given by the energy transport velocity [14] for a time-harmonic field. For such an ultrashort Gaussian pulse this point in the field evolution may not correspond to the space-time point at which the peak amplitude in the propagated fields occurs ($\approx \theta_0$), as seen in Fig. 3, which propagates with a velocity $v_B \cong c/\theta_0$ that is nearly independent of the carrier frequency ω_c. Finally, in the extremely ultrashort-pulse limit when the Sommerfeld precursor field $A_S(z,t)$ is also excited with sufficient amplitude, a separate peak amplitude will also appear at a very high oscillation frequency (well above the medium resonance frequency), and this point will propagate at a velocity v_{SF} that is just below the vacuum speed of light c.

For $(\omega_0^2 - \delta^2)^{1/2} < \omega_c \leq (\omega_1^2 - \delta^2)^{1/2}$, so that the input signal frequency is within the absorption band of the medium, the same general dynamical field evolution is obtained as in the below resonance case with two important modifications. First of all, the Sommerfeld precursor $A_S(z,t)$ becomes more pronounced as ω_c increases from ω_0 to ω_1, as seen from a comparison of Figs. 6 and 9. Second, the instantaneous frequency of oscillation of the propagated field in the mature-dispersion regime only approaches the input signal frequency ω_c for an ultrashort pulse, as seen in Figs. 8 and 11, and as it does, the field amplitude rapidly attenuates from the peak amplitude attained at either a lower oscillation frequency in the Brillouin precursor or a higher oscillation frequency in the Sommerfeld precursor. Because the input signal frequency ω_c for the case illustrated in Figs. 6–8 is at the lower end of the absorption band, the Brillouin precursor dominates the Sommerfeld precursor at all propagation distances. The peak amplitude in the propagated field then occurs immediately following the point $t = \theta_0 z/c$, at which point the oscillation frequency is zero, after which the field amplitude rapidly diminishes as the oscillation frequency approaches ω_0 from below. The total field evolution when the input signal frequency is near the upper end of the absorption band is illustrated in Figs. 9–11 for an initial Gaussian-pulse width $2T = 2.0 \times 10^{-16}$ sec and carrier frequency $\omega_c = 5.75 \times 10^{16}$/sec. The dynamical field evolution for this case is illustrated in Figs. 15–20 at several values of the propagation distance in the mature-dispersion regime. This case is of particular interest since the group velocity at this signal frequency is very nearly equal to the vacuum speed of light c. At a small propagation distance the peak amplitude in the temporal field evolution occurs during the generalized Sommerfeld precursor evolution as seen in Fig. 9, and this point propagates with a velocity just below c. However, the frequency of oscillation about this point is much larger than ω_c. As the propagation distance increases, as shown in Figs. 15–20, the total field evolution becomes increasingly dominated by the generalized Brillouin precursor whose peak amplitude point propagates with a velocity approximately equal to $c/\theta_0 = c/n(0)$; however, the oscillation frequency of the field about this point is much less than the initial signal frequency ω_c. It may, perhaps, be a moot point that the oscillation frequency of the propagated field due to an ultrashort Gaussian pulse in the mature-dispersion regime of the medium absorption band never reaches the input signal frequency $\omega_c \in [(\omega_0^2 - \delta^2)^{1/2}, (\omega_1^2 - \delta^2)^{1/2}]$ since the field amplitude is exponentially negligible as the oscillation frequency approaches either $(\omega_0^2 - \delta^2)^{1/2}$ from below (due to the Brillouin precursor) or $(\omega_1^2 - \delta^2)^{1/2}$ from above (due to the

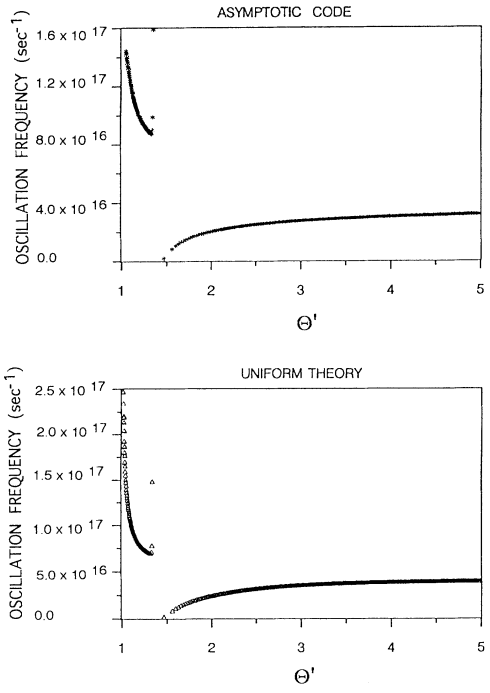

FIG. 20. Evolution of the instantaneous angular frequency of oscillation for the dynamical field evolution due to an input Gaussian-modulated cosine field with initial pulse width $2T = 0.2$ fsec and a carrier frequency $\omega_c = 5.75 \times 10^{16}$ sec^{-1} at a propagation distance $z = 419.60 z_d$, where z_d is the absorption depth at the carrier frequency ω_c. The asterisks in the top diagram denote the frequency of oscillation values that were determined from the asymptotic code, while the triangles in the bottom diagram denote the frequency of oscillation values that were determined from the uniform theory.

Sommerfeld precursor). Finally, if one only considered the propagated envelope of this field evolution it would easily be concluded that the input Gaussian pulse has, under propagation, separated into two distinct pulses, the first pulse having a peak amplitude that propagates just below c and the second pulse having a peak amplitude that propagates at the velocity $v_B \cong c/\theta_0$.

Finally, for $\omega_c > (\omega_1^2 - \delta^2)^{1/2}$ the Sommerfeld precursor $A_S(z,t)$ will dominate the propagated-field behavior in the mature-dispersion regime, as illustrated in Figs. 12–14 for an input Gaussian-pulse width $2T = 2.0 \times 10^{-16}$ sec with signal frequency $\omega_c = 10.0 \times 10^{16}$/sec at the propagation distance $z = 15.09 z_d$. The value $\theta_c \cong 1.2002$ in Fig. 14 indicates the point in the field evolution at which the oscillation frequency equals ω_c; for $\theta' < \theta_c$ the instantaneous oscillation frequency of $A(z,t)$ is greater than ω_c, while for $\theta' > \theta_c$ it is less than ω_c. It is about this point that the Gaussian factor peaks to its maximum value. However, because the attenuation of the Sommerfeld precursor identically vanishes at $\theta' = 1$ while it monotonically increases for all $\theta' > 1$, the peak in the propagated field is shifted toward this space-time point. Notice that the peak amplitude of the generalized Brillouin precursor that is present in the propagated-field structure is reduced by a factor of 10^{-7} from that of the Sommerfeld precursor in this case. As the initial pulse width is decreased the relative amplitude of the Brillouin precursor field increases with respect to that of the Sommerfeld precursor and in the limit the entire field evolution approaches that due to an input δ-function pulse. On the other hand, as the initial pulse width is increased the amplitude of the Brillouin precursor field decreases and only the generalized Sommerfeld precursor remains as the spectral amplitude approaches zero everywhere except in a small neighborhood of ω_c. In each case, the point in the field evolution of a short Gaussian pulse at which the oscillation frequency passes through ω_c is given by the value $\theta_c \cong \theta_E$.

The signal velocity for a short Gaussian pulse is then seen to be given approximately by the energy velocity for a time-harmonic field in the dispersive medium

$$v_S \cong v_E(\omega_c) \tag{4.6}$$

for $0 \leq \omega_c < (\omega_0^2 - \delta^2)^{1/2}$ and $\omega_c > (\omega_1^2 - \delta^2)^{1/2}$. This is the same as the signal velocity for both the unit-step-function modulated and rectangular-function modulated signals below resonance and is an upper envelope to the signal velocity above the absorption band [4,5]. The signal velocity of an ultrashort Gaussian pulse with signal frequency ω_c within the medium absorption band is not defined since the oscillation frequency of the propagated field only approaches ω_c in the mature-dispersion regime. As the initial pulse width is broadened into the quasimonochromatic regime where the initial pulse spectrum is sharply defined about the signal frequency ω_c, it is expected that the signal velocity will remain to be given approximately by the monochromatic energy transport velocity $v_E(\omega_c)$, even for frequencies in the medium absorption band. This transition between the ultrashort and quasimonochromatic regimes needs to be carefully considered in future research.

V. CONCLUSIONS

The results presented here clearly show that the asymptotic theory provides a complete, accurate description of ultrashort Gaussian-pulse propagation in a causally dispersive dielectric as described by the Lorentz model. The only significant source of error in the asymptotic theory arises from the analytic approximations to the relevant saddle-point dynamics. Although these algebraic approximations were sufficiently accurate for the asymptotic description of the propagated-pulse evolution due to either an input step-function modulated signal, a rectangular envelope pulse, or a δ-function pulse [4–6], they were found here to be inadequate for the case of an input Gaussian pulse due to the exponential behavior of the initial pulse envelope spectrum. Nevertheless, the analytical asymptotic theory was found to be qualitatively correct in its description of Gaussian-pulse propagation [29]. The inclusion of the correct, numerically determined saddle-point dynamics then brings the asymptotic theory into complete quantitative agreement with the numerical experiments, as has been clearly shown here.

When combined with previously published results [5–11], the results presented here clearly show that the precursor fields are critical for the complete understanding of the dispersive pulse dynamics in a causal medium. For a single-resonance Lorentz medium, as considered here, these are the classical Sommerfeld and Brillouin precursors [1–3], whose complete dynamics [5] and uniform asymptotic description [6] have only recently been obtained and provided with a proper physical interpretation [12]. For a multiple-resonance Lorentz medium additional precursor fields may also be present [8], which will further enrich the observed pulse evolution. For an instantaneous rise-time pulse of arbitrary initial width (such as that given by a rectangular envelope) the resultant pulse distortion was found [9] to be primarily due to the interference between the precursor fields associated with the leading and trailing edges of the input pulse. For a more continuous initial pulse envelope whose spectrum is an entire function of complex ω, such as that presented by a Gaussian envelope as considered here, the entire propagated field is found to be given by the superposition of the so-called generalized precursor fields, whose evolution is dictated by the saddle-point dynamics. For an ultrashort pulse with initial rise time $T \leq 1/\delta$, the saddle-point dynamics depend primarily on the properties of the dispersive medium. An input Gaussian pulse can then evolve into a pair of pulses in a single-resonance Lorentz medium for a sufficiently short initial pulse width. In a double-resonance Lorentz medium a maximum of three pulses is possible.

Finally, the signal velocity $v_c(\omega_c)$ of an ultrashort Gaussian pulse in a single-resonance Lorentz medium is found to be given approximately by the monochromatic energy transport velocity $v_E(\omega_c)$ due to London [14]. The signal velocity v_c marks the point in the field evolution that oscillates at the input carrier frequency. The

signal velocity for an ultrashort Gaussian pulse differs, in general, from the velocity of the peak amplitude point appearing in the propagated field in the mature-dispersion regime, which propagates either very near to the vacuum speed of light c if the generalized Sommerfeld precursor dominates the field or near $c/n(0)$ if the generalized Brillouin precursor dominates the propagated-field structure. As the initial pulse width is initially broadened, the signal velocity v_c is found to decrease away from $v_E(\omega_c)$ so that v_E is an upper envelope to the signal velocity for the ultrashort Gaussian pulse, just as it is an upper envelope for the unit-step-function signal and the rectangular envelope pulse. As the initial pulse rise time T is significantly increased above $1/\delta$, it is expected that the signal velocity will approach $v_E(\omega_c)$ from below. This transition from the ultrashort to the quasimonochromatic pulse regime is a critical topic for future research.

ACKNOWLEDGMENT

The research presented in this paper was supported by the Applied Mathematics Group of the United States Air Force Office of Scientific Research under Contract No. F49620-89-C-0057 and Grant No. F49620-92-J-0206.

[1] A. Sommerfeld, Ann. Phys. **44**, 177 (1914).
[2] L. Brillouin, Ann. Phys. **44**, 203 (1914).
[3] L. Brillouin, *Wave Propagation and Group Velocity* (Academic, New York, 1960).
[4] K. E. Oughstun, Ph.D. dissertation, University of Rochester, 1978, available from University Microfilms International, Ann Arbor, MI.
[5] K. E. Oughstun and G. C. Sherman, J. Opt. Soc. Am. B **5**, 817 (1988).
[6] K. E. Oughstun and G. C. Sherman, J. Opt. Soc. Am. A **6**, 1394 (1989).
[7] K. E. Oughstun, Proc. IEEE **79**, 1379 (1991).
[8] S. Shen and K. E. Oughstun, J. Opt. Soc. Am. B **6**, 948 (1989).
[9] K. E. Oughstun and G. C. Sherman, Phys. Rev. A **41**, 6090 (1990).
[10] P. Wyns, D. P. Foty, and K. E. Oughstun, J. Opt. Soc. Am. A **6**, 1421 (1989).
[11] K. E. Oughstun, P. Wyns, and D. P. Foty, J. Opt. Soc. Am. A **6**, 1430 (1989).
[12] G. C. Sherman and K. E. Oughstun, Phys. Rev. Lett. **47**, 1451 (1981).
[13] I. Tolstoy, *Wave Propagation* (McGraw-Hill, New York, 1973), Chaps. 1 and 2.
[14] R. Loudon, J. Phys. **3**, 233 (1970).
[15] K. E. Oughstun and S. Shen, J. Opt. Soc. Am. B **5**, 2395 (1988).
[16] R. L. Fork, C. H. Brito Cruz, P. C. Becker, and C. V. Shank, Opt. Lett. **12**, 483 (1987).
[17] C. G. B. Garrett and D. E. McCumber, Phys. Rev. A **1**, 305 (1970).
[18] J. Jones, Am. J. Phys. **42**, 43 (1974).
[19] D. G. Anderson and J. H. Askne, Proc. IEEE **62**, 1518 (1974).
[20] D. Anderson, J. Askne, and M. Lisak, Phys. Rev. A **12**, 1546 (1975).
[21] D. Anderson and M. Lisak, Phys. Rev. A **35**, 184 (1987).
[22] N. D. Hoc, I. M. Besieris, and M. E. Sockell, IEEE Trans. Antennas Propag. **AP-33**, 1237 (1985).
[23] I. P. Christov, IEEE J. Quantum Electron. **QE-24**, 1548 (1988).
[24] H. M. Nussenzveig, *Causality and Dispersion Relations* (Academic, New York, 1972), Chap. 1.
[25] M. D. Crisp, Phys. Rev. A **1**, 1604 (1970).
[26] R. Barakat, J. Opt. Soc. Am. B **3**, 1602 (1986).
[27] D. B. Trizna and T. A. Weber, Radio Sci. **17**, 1169 (1982).
[28] J. A. Stratton, *Electromagnetic Theory* (McGraw-Hill, New York, 1941), Sec. 5-18.
[29] K. E. Oughstun and J. E. K. Laurens, Radio Sci. **26**, 245 (1991).
[30] T. Hosono, in *Proceedings of the 1980 International URSI Symposium on Electromagnetic Waves* (International Union of Radio Science, Munich, 1980), paper 112, pp. C1–C4.
[31] E. T. Copson, *Asymptotic Expansions* (Cambridge University Press, Cambridge, England, 1965), Chaps. 7–9.
[32] F. W. J. Olver, Stud. Appl. Math. Rev. **12**, 228 (1970).
[33] R. A. Handelsman and N. Bleistein, Arch. Ration. Mech. Anal. **35**, 267 (1969).
[34] C. Chester, B. Friedman, and F. Ursell, Proc. Cambridge Philos. Soc. **53**, 599 (1957).
[35] *Handbook of Mathematical Functions,* Natl. Bur. Stand. Appl. Math. Ser. No. 55, edited by M. Abramowitz and I. A. Stegun (U.S. GPO, Washington, D.C., 1972).
[36] I. P. Christov, in *Generation and Propagation of Ultrashort Optical Pulses,* edited by E. Wolf, Progress in Optics Vol. XXIX (Elsevier, Amsterdam, 1991), Chap. 3.